THE JOURNAL OF BIOLOGICAL CHEMISTRY VOL. 291, NO. 45, pp. 23589–23603, November 4, 2016

Bypass of DNA-Protein Cross-links Conjugated to the 7-Deazaguanine Position of DNA by Translesion Synthesis Polymerases*[S]

Received for publication, June 29, 2016, and in revised form, August 24, 2016 Published, JBC Papers in Press, September 12, 2016, DOI 10.1074/jbc.M116.745257

Susith Wickramaratne[‡§], Shaofei Ji[‡§], Shivam Mukherjee[¶], Yan Su[‖], Matthew G. Pence[‖1], Lee Lior-Hoffmann[**], Iwen Fu[**], Suse Broyde[**], F. Peter Guengerich[‖], Mark Distefano[§], Orlando D. Schärer[¶‡‡], Yuk Yin Sham[§§], and Natalia Tretyakova[‡¶¶2]

From the [‡]Masonic Cancer Center and the [§]Departments of Chemistry, [§§]Center for Drug Design and [¶¶]Medicinal Chemistry, University of Minnesota, Minneapolis, Minnesota 55455, [‡‡]Departments of Pharmacological Sciences and [¶]Chemistry, Stony Brook University, Stony Brook, New York 11794, [**]Department of Biology, New York University, New York, New York 10003-6688, and [‖]Department of Biochemistry, Vanderbilt University School of Medicine, Nashville, Tennessee 37232

DNA-protein cross-links (DPCs) are bulky DNA lesions that form both endogenously and following exposure to bis-electrophiles such as common antitumor agents. The structural and biological consequences of DPCs have not been fully elucidated due to the complexity of these adducts. The most common site of DPC formation in DNA following treatment with bis-electrophiles such as nitrogen mustards and cisplatin is the N7 position of guanine, but the resulting conjugates are hydrolytically labile and thus are not suitable for structural and biological studies. In this report, hydrolytically stable structural mimics of *N*7-guanine-conjugated DPCs were generated by reductive amination reactions between the Lys and Arg side chains of proteins/peptides and aldehyde groups linked to 7-deazaguanine residues in DNA. These model DPCs were subjected to *in vitro* replication in the presence of human translesion synthesis DNA polymerases. DPCs containing full-length proteins (11–28 kDa) or a 23-mer peptide blocked human polymerases η and κ. DPC conjugates to a 10-mer peptide were bypassed with nucleotide insertion efficiency 50–100-fold lower than for native G. Both human polymerase (hPol) κ and hPol η inserted the correct base (C) opposite the 10-mer peptide cross-link, although small amounts of T were added by hPol η. Molecular dynamics simulation of an hPol κ ternary complex containing a template-primer DNA with dCTP opposite the 10-mer peptide DPC revealed that this bulky lesion can be accommodated in the polymerase active site by aligning with the major groove of the adducted DNA within the ternary complex of polymerase and dCTP.

Covalent entrapment of cellular proteins on genomic DNA is a common process that occurs upon exposure to a variety of endogenous and exogenous bis-electrophiles, heavy metals, and free radicals (1–7). Specifically, common chemotherapeutics such as nitrogen mustards, platinum compounds, and alkylnitrosoureas (3, 4, 8); environmental carcinogens such as formaldehyde and 1,3-butadiene (5, 9, 10); toxic metals (11–13); nitric oxide (14); free radicals (15, 16); UV light (17); and ionizing radiation (6) mediate the formation of covalent DNA-protein cross-links (DPCs).[3] Mass spectrometry-based proteomic studies have identified a large number of cellular proteins that participate in DPC formation in cells treated with cross-linking agents, including DNA repair proteins, DNA polymerases, transcription factors, and structural proteins such as histones, heat shock proteins, and tubulins (3–6, 8, 10).

Because of their enormous size as compared with other nucleobase lesions and their ability to disrupt DNA duplex structure and DNA-protein interactions, DPCs are hypothesized to interfere with DNA replication and transcription (1, 2). We reported previously that protein monoepoxide reagents that selectively induce DPC lesions cause toxicity and mutations in human cells (18). In a more recent study, we have shown that human cells deficient in nucleotide excision repair were sensitized toward nitrogen mustard toxicity and contained increased numbers of *N*7-guanine-conjugated DPC lesions (19). Covalent DPCs have been detected in peripheral blood lymphocytes from breast cancer patients undergoing treatment with cyclophosphamide.[4] Recent studies by Jentsch and co-workers (20, 21) and Walter and co-workers (22) have provided evidence that DPCs are subject to proteolytic cleavage to the corresponding DNA-peptide lesions, which are subsequently removed from DNA in a replication-dependent repair process. Thus, it is critically important to investigate the activ-

* This work was supported by National Institutes of Health NIEHS Grants R01 ES023350 (to N. T.), R01 ES010546 (to F. P. G.), and R01 ES025987 (to S. B.); NCI, National Institutes of Health Grants R01 CA100670 (to N. T.) and R01 CA75449 (to S. B.); and NIGMS, National Institutes of Health Grant R01 GM084152 (to M. D.) and a Brainstorm Award from the University of Minnesota Masonic Cancer Center. The authors declare that they have no conflicts of interest with the contents of this article. The content is solely the responsibility of the authors and does not necessarily represent the official views of the National Institutes of Health.

[S] This article contains a supplemental movie.

[1] Present address: J. R. Simplot Co., Plant Sciences, 5369 W. Irving St., Boise, ID 83706.

[2] To whom correspondence should be addressed: University of Minnesota Masonic Cancer Center, 2231 6th St. S.E., 2-147 CCRB, Minneapolis, MN 55455. Tel.: 612-626-3432; Fax: 612-624-3869; E-mail: trety001@umn.edu.

[3] The abbreviations used are: DPC, DNA-protein cross-link; TLS, translesion synthesis; ESI, electrospray ionization; eGFP, enhanced GFP; RMSD, root mean square deviation; RMSF, root mean square fluctuation; hPol, human polymerase; deaza-DHP-dG, 7-deaza-7-(2,3-dihydroxypropan-1-yl)-2′-deoxyguanosine; Pol, polymerase; dmf, dimethylformadine; CE, cyanoethyl; CPG, controlled pore glass; PNK, polynucleotide kinase; FAM, fluorescein amidite; MD, molecular dynamics.

[4] A. Groehler and N. Tretyakova, unpublished observations.

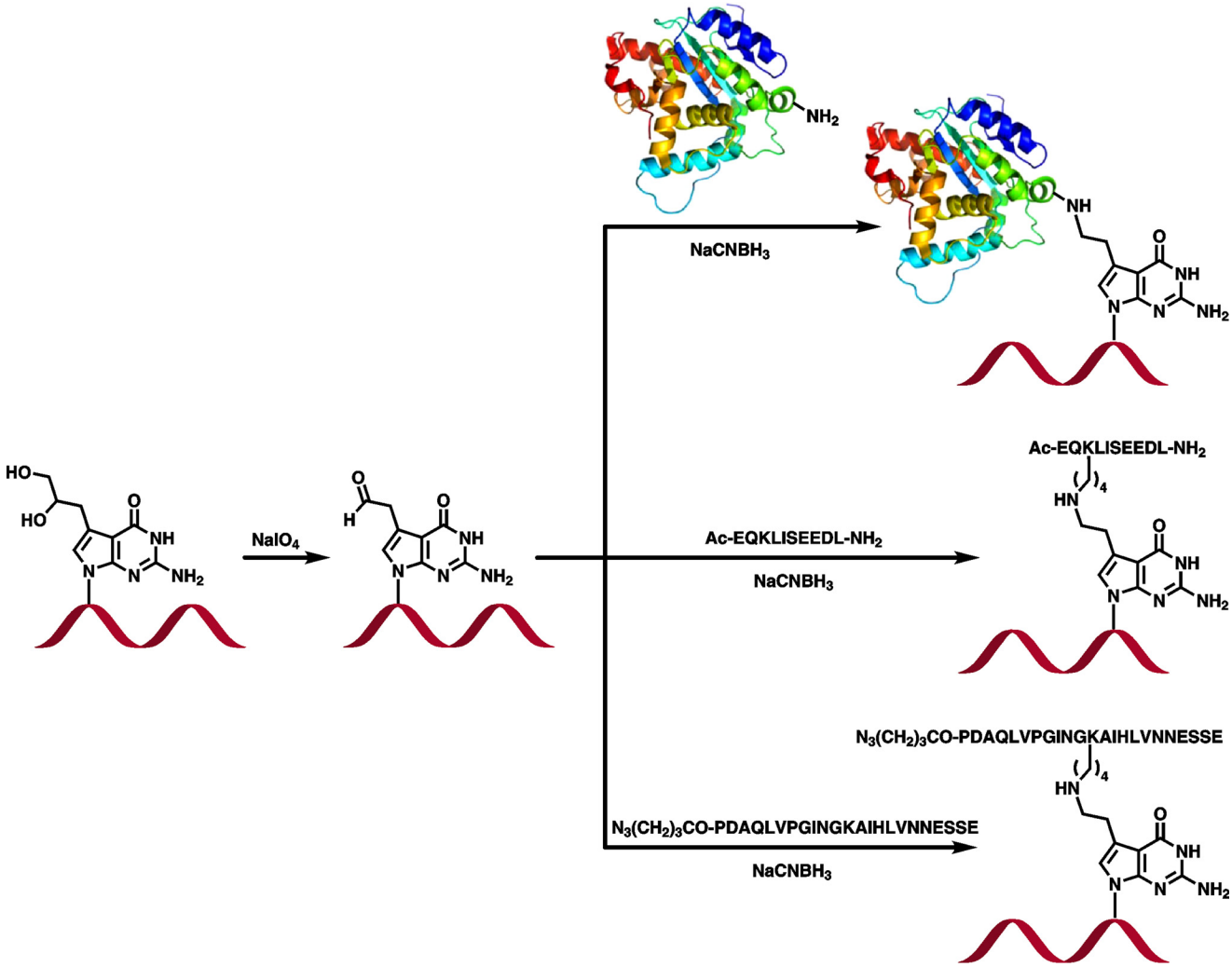

FIGURE 1. **Synthesis of DNA-protein and DNA-peptide cross-links by postsynthetic reductive amination.**

ity and accuracy of DNA polymerases on DNA-protein and DNA-peptide lesions.

The most common site on DNA that participates in DNA-protein cross-linking mediated by bis-electrophiles is the N7 atom of guanine (3–5, 10). However, to our knowledge, no reports are available in the literature in regard to the replication bypass of *N*7-guanine adducts, probably because of their labile nature. Alkylation at the N7 atom of 2′-deoxyguanosine creates a positive charge at the affected nucleobase, destabilizing the *N*-glycosidic bond and leading to spontaneous depurination and abasic site formation (23, 24).

In the present work, we generated a range of hydrolytically stable model DPCs structurally resembling *N*7-guanine cross-links. Template-primer complexes containing model DPCs were subjected to *in vitro* polymerization in the presence of human lesion bypass DNA polymerases under steady-state kinetic conditions, and the resulting primer extension products were characterized by gel electrophoresis and HPLC-ESI-MS/MS. Finally, molecular dynamics (MD) simulations were conducted to examine how DNA-peptide lesions can be accommodated within the active site of human lesion bypass polymerase κ.

Results

Synthesis and Characterization of DNA-Protein and DNA-Peptide Cross-links—Model DNA-protein and DNA-peptide conjugates were prepared by reductive amination reactions between the Lys/Arg side chains of proteins/peptides and 7-deaza-7-(2-oxoethyl)-2′-deoxyguanosine of DNA (Fig. 1). The latter were formed *in situ* from 7-deaza-7-(2,3-dihydroxypropan-1-yl)-2′-deoxyguanosine-containing DNA as described in our earlier publication (25). In the resulting model cross-links, Lys or Arg side chains of proteins and peptides are conjugated to the 7-deazaguanine residues of DNA via a two-carbon linker, creating a structure that is analogous to DPC lesions induced in cells by antitumor nitrogen mustards (3) and ethylene dibromide (26).

DNA sequences (5′-G TCA CTG GTA *X*CA AGC ATT G-3′ and 5′-GAA AGA AG*X* ACA GAA GAG GGT ACC ATC ATA GAG TCA GTG-3′ where *X* is the modified base; Table 1) were selected to minimize self-annealing and were used previously in studies of DNA-DNA cross-links (27, 28). Two peptides of increasing size, a 10-mer peptide derived from c-Myc protein (EQKLISEEDL) and a 23-mer derived from tetanus toxoid

TABLE 1
Synthetic DNA sequences used in the present study
X is dG, 7-DHP-7-deaza-dG, or DPC as indicated.

Abbreviation	Sequence
P1	5′-CAA ***FAMT***GC TTG-3′
P2	5′-CTA TGA ***FAMT***GG TAC C-3′
P3	^{32}P-5′-CAA TGC TTG-3′
P4	Biotin-5′-T_{10}-CAA TGC UTG-3′
T1	5′-G TCA CTG GTA GCA AGC ATT G-3′
T2	5′-G TCA CTG GTA ***X***CA AGC ATT G-3′ (*X* = deaza-DHP-dG)
T3	5′-G TCA CTG GTA ***X***CA AGC ATT G-3′ (*X* = N_3 $(CH_2)_3$CO-EQKLISEEDL-NH_2)
T4	5′-G TCA CTG GTA ***X***CA AGC ATT G-3′ (*X* = Ac-EQKLISEEDL-NH_2)
T5	5′-G TCA CTG GTA ***X***CA AGC ATT G-3′ (*X* = azido- $(CH_2)_3$CO-PDAQLVPGINGKAIHLVNNESSE)
T6	5′-G TCA CTG GTA ***X***CA AGC ATT G-3′ (*X* = AlkB protein)
T7	5′-G TCA CTG GTA ***X***CA AGC ATT G-3′ (*X* = histone H4)
T8	5′-G TCA CTG GTA ***X***CA AGC ATT G-3′ (*X* = histone H2A)
T9	5′-G TCA CTG GTA ***X***CA AGC ATT G-3′ (*X* = eGFP)
T10	5′-GAA AGA AGG ACA GAA GAG GGT ACC ATC ATA GAG TCA GTG-3′
T11	5′-GAA AGA AG***X*** ACA GAA GAG GGT ACC ATC ATA GAG TCA GTG-3′ (*X* = deaza-DHP-dG)
T12	5′-GAA AGA AG***X*** ACA GAA GAG GGT ACC ATC ATA GAG TCA GTG-3′ (*X* = N_3 $(CH_2)_3$CO-EQKLISEEDL-NH_2)
T13	5′-GAA AGA AG***X*** ACA GAA GAG GGT ACC ATC ATA GAG TCA GTG-3′ (*X* = N_3 $(CH_2)_3$CO-PDAQLVPGINGKAIHLVNNESSE)
T14	5′-GAA AGA AG***X*** ACA GAA GAG GGT ACC ATC ATA GAG TCA GTG-3′ (*X* = AlkB protein)
T15	5′-GAA AGA AG***X*** ACA GAA GAG GGT ACC ATC ATA GAG TCA GTG-3′ (*X* = histone H4)
T16	5′-GAA AGA AG***X*** ACA GAA GAG GGT ACC ATC ATA GAG TCA GTG-3′ (*X* = eGFP)

($N_3(CH_2)_3$CO-PDAQLVPGINGKAIHLVNNESSE) were used. The same two peptides were used in our earlier publication investigating replication bypass of DPCs conjugated to the C5 position of thymidine using Cu(I)-catalyzed azide-alkyne cycloaddition (29). In addition, histone H2A (14 kDa), histone H4 (11.5 kDa), and AlkB (22.9 kDa) were chosen for these experiments based on the documented ability of histones and DNA repair proteins to engage in the formation of DNA-protein cross-links (3, 4, 8, 10). We also included enhanced green fluorescent protein (eGFP; 28 kDa), which was used in our earlier study of pyrimidine-conjugated DPCs (29). DNA-peptide and DNA-protein conjugates were isolated by gel electrophoresis, and their purity was confirmed by PAGE (see representative gel image in Fig. 2). Synthetic DNA-protein and DNA-peptide cross-links were structurally characterized by nano-HPLC-nanoelectrospray ionization-MS/MS (25).

Replication Bypass of DNA-Protein Cross-links—To examine the influence of DNA-protein cross-links conjugated to the C7 position of 7-deaza-G in DNA on DNA replication, template-primer complexes containing site-specific DPC lesions (10-mer peptide EQKLISEEDL derived from c-Myc protein (30, 31), 23-mer peptide PDAQLVPGINGKAIHLVNNESSE derived from tetanus toxoid, AlkB, histones H4 and H2A, and GFP protein) were subjected to standing start and running start primer extension in the presence of human translesion synthesis (TLS) polymerases η and κ. Templates containing native dG and deaza-DHP-dG served as negative controls.

Our "standing start" assays used a 9-mer primer P1 (5′-CAA ***FAMT***GC TTG-3′) extending to the penultimate position of the modified site (−1 primer) on the 20-mer templates T1–T9 (5′-G TCA CTG GTA ***X***CA AGC ATT G-3′ where *X* is unmodified dG, deaza-DHP-dG, or a DPC adduct; Table 1 and Fig. 3*A*). Standing start primer extension past dG- and deaza-DHP-dG-containing templates resulted in complete extension products (20-mers) by hPols η and κ (Figs. 4, *A* and *B*, and 5, *A* and *B*). We found that the 10-mer peptide DPC was bypassed by hPols η and κ albeit with low efficiencies (Figs. 4*C* and 5*C*). In contrast, the 23-mer peptide cross-link and all three protein conjugates completely blocked primer extension (Figs. 4, *D–G*, and 5, *D–F*). The ability of polymerase η to copy the damaged strand was restored when the protein portion of DPC was digested with proteinase K (Fig. 4*H*). Taken together, these results indicate that the ability of TLS polymerases to bypass DPC lesions is a function of peptide size with lesions ≥23 amino acids long causing a complete replication block.

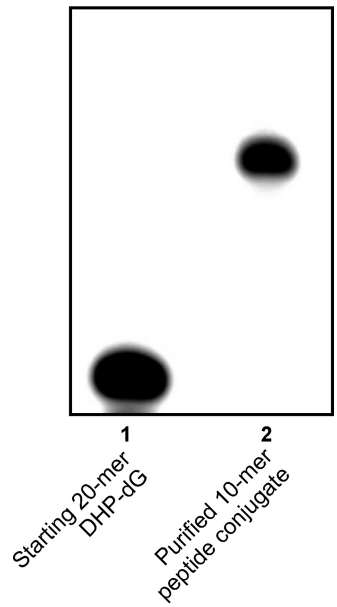

FIGURE 2. **Representative purity check for a DNA-peptide conjugate (5′-G TCA CTG GTA *X*CA AGC ATT G-3′ where *X* is conjugated to EQKLISEEDL via the Lys residue.**

Because bulky DPC lesions may affect polymerase loading on the primer, *in vitro* replication experiments were repeated under "running start" conditions. Running start experiments were conducted using 13-mer primer P2 (5-CTA TGA ***FAMT***GG TAC C-3) annealed to 39-mer templates T10–T16 (5′-GAA AGA AG***X*** ACA GAA GAG GGT ACC ATC ATA GAG TCA GTG-3′ where *X* is unmodified dG, deaza-DHP-dG, or DNA-protein conjugate; Table 1 and Fig. 3*B*). In this primer-template complex, the 3′-end of the primer is placed 10 nucleotides upstream from the adducted site (−10 primer; Fig. 3*B*).

A. 5'-CAA ***FAMT*** GC TTG -3' (9-mer FAMdT primer)
3'-GTT ACG AAC ***X***AT GGT CAC TG-5' (20-mer template)

B. 5'-C TAT GA***FAMT*** GGT ACC -3' (13-mer FAMdT primer)
3'-GTG ACT GAG ATA CT A CCA TGG GAG AAG ACA ***X***GA AGA AAG-5' (39-mer template)

C. ^{32}P-5'-CAA TGC TTG -3' (9-mer primer)
3'-GTT ACG AAC ***X***AT GGT CAC TG-5' (20-mer template)

D. Biotin-5'-$(T)_{10}$-CAA TGC UTG -3' (19-mer primer)
3'-GTT ACG AAC ***X***AT GGT CAC TG-5' (20-mer template)

FIGURE 3. **Sequences of DNA oligomers used in this study.** *A*, 9-mer FAMdT primer-20-mer template duplex used in standing start assays; *B*, 13-mer FAMdT primer-39-mer template DNA duplex used in running start assays; *C*, 9-mer primer-20-mer template duplex used for the single nucleotide incorporation and steady-state kinetic assays; *D*, biotinylated 19-mer primer-20-mer template duplexes used for the LC-MS/MS analyses of primer extension products. *X* = dG, 7-DHP-7-deaza-dG, or DPC.

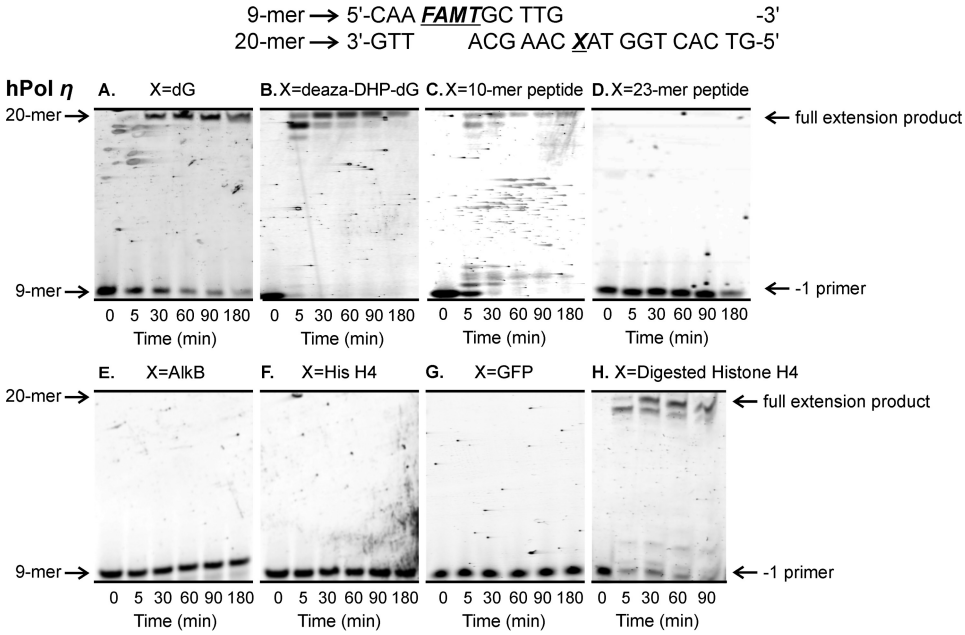

FIGURE 4. **Standing start assays for replication bypass of DNA-peptide and DNA-protein cross-links by hPol η.** 9-mer FAMdT primers were annealed with 20-mers containing unmodified dG (*A*), deaza-DHP-dG (*B*), or covalent cross-links to 10-mer peptide EQKLISEEDL (*C*), 23-mer peptide PDAQLVPGINGKAIHLVNNESSE (*D*), or full-sized protein AlkB (*E*), histone (*His*) H4 (*F*), or eGFP (*G*). The resulting primer-template duplexes (0.15 μM) were incubated in the presence of hPol η (0.30 μM). Reactions were initiated by the addition of a mixture of dNTPs (500 μM) and quenched at the indicated time points. Extension products were separated by 20% denaturing PAGE and visualized by fluorescence imaging. *Panel H* shows results for DPC to histone (*His*) H4 following digestion with Proteinase K.

We found that under running start conditions, both 10-mer and 23-mer peptide conjugates were partially bypassed by hPols η and κ to generate full-length products. For both peptide lesions, pronounced pausing was observed 1–2 nucleotides ahead of the adducted site and downstream from the lesion, suggesting inefficient polymerase translocation along the template (Figs. 6, *C* and *D*, and 7, *C* and *D*). Although the deaza-DHP-dG control caused some degree of polymerase pausing, it was less blocking than the peptide lesions (Figs. 6*B* and 7*B*). In contrast, all three DPC lesions completely blocked nucleotide addition, yielding no extension products (Figs. 6, *E*–*G*, and 7*E*). Similar results were observed when the primer was moved farther upstream from the lesion site (Fig. 8). As was the case with standing start experiments, proteinase K-digested cross-links were bypassed (Fig. 6*H*). Interestingly, replication past proteinase K-digested lesions and peptide cross-links generated large numbers of −3, −2, and −1 products (Fig. 6, *C*, *D*, and *H*). Taken together, our running start experiments are consistent with the standing start results (Figs. 4 and 5), indicating that although peptide DPCs can be bypassed by TLS polymerases η and κ DPCs to full-length proteins completely block DNA replication. In cells, such replication blockage may be relieved by proteolytic degradation of the protein component of DPC (20–22).

Kinetics of Single Nucleotide Incorporation Opposite 10-mer Peptide Cross-link—To examine the fidelity of nucleotide insertion opposite DNA-peptide lesions by TLS polymerases, single nucleotide insertion assays were conducted. Template-primer complexes created by annealing radiolabeled 9-mer primers (^{32}P-5′-CAA TGC TTG-3′) to 20-mer templates (5′-G TCA CTG GTA ***X***CA AGC ATT G-3′; Fig. 3*C*) were incubated with hPol η or κ in the presence of individual dNTPs (100 μM) for 0–60 min. Denaturing PAGE-phosphorimaging analyses revealed that both polymerases preferentially incorporated the

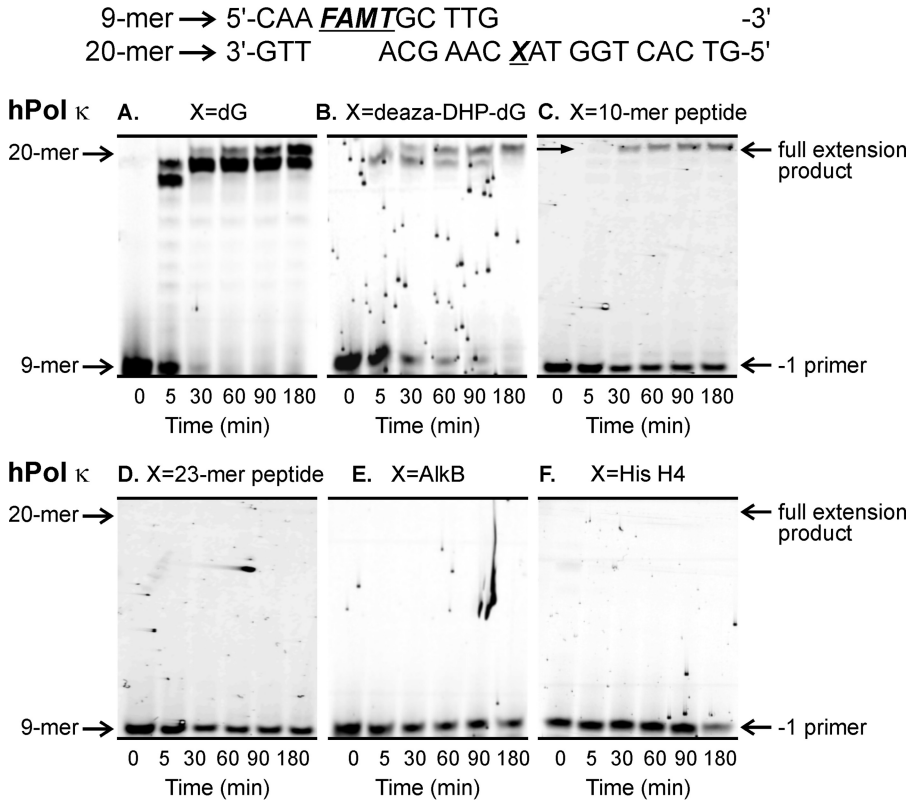

FIGURE 5. **Standing start assays for replication bypass of DNA-protein cross-links by hPol κ.** 9-mer FAMdT primers were annealed with 20-mers containing unmodified dG (*A*), deaza-DHP-dG (*B*), or covalent cross-links to 10-mer peptide EQKLISEEDL (*C*), 23-mer peptide PDAQLVPGINGKAIHLVNNESSE (*D*), or full-sized protein AlkB (*E*) or histone (*His*) H4 (*F*). The resulting primer-template duplexes (0.15 μM) were incubated in the presence of hPol κ (0.30 μM). Reactions were initiated by the addition of a mixture of dNTPs (500 μM) and quenched at the indicated time points. Extension products were separated by 20% denaturing PAGE and visualized by fluorescence imaging.

correct base (dC) opposite native G as expected (see representative data in Figs. 9 and 10). Furthermore, hPol κ inserted a single nucleotide opposite the 10-mer peptide cross-link with high fidelity (Fig. 10). hPol η also favored the incorporation of the correct base (C), although a small amount of T was also incorporated (Fig. 9).

To determine the catalytic efficiency and to calculate the misinsertion frequency for incorporation of individual dNTPs opposite the 10-mer peptide cross-link, primer-template duplexes containing unmodified dG or 10-mer peptide cross-link (Fig. 3*C*) were incubated with hPol η or κ in the presence of increasing concentrations of individual dNTPs (0–500 μM), and the reactions were quenched at preselected time points (0–60 min). Polymerase concentrations and the time points were selected such that the extent of product formation was <35% of the starting substrate concentration (see representative gel image in Fig. 11). The specificity constant (k_{cat}/K_m) was calculated to evaluate the catalytic efficiency of incorporation of each dNTP and the frequency of incorporating an incorrect *versus* correct dNTP opposite the lesion (*f*) (32) were calculated by plotting the reaction velocity against dNTP concentration.

Our steady-state kinetic studies have revealed that the specificity constants (k_{cat}/K_m) for nucleotide insertion by hPol η were 4–150-fold higher compared with those of hPol κ, indicating that replication of DNA-peptide lesions is more efficient in the presence of hPol η (Table 2). The specificity constants for the insertion of the correct base (dCTP) opposite the adduct were 0.03 and 0.0002 μM^{-1} min^{-1} for hPols η and κ, respectively (Table 2). These values were 49- and 1850-fold lower than those obtained for dCTP insertion opposite native G (1.5 and 0.37 μM^{-1} min^{-1}, respectively, Table 2), reflecting the difficulty of accommodating the bulky peptide adduct in the polymerase active site.

Nucleotide insertion opposite the 10-mer peptide conjugate by hPols η and κ was characterized by high fidelity, resulting in incorporation of C opposite the adduct. The insertion frequency of dTMP (*f*) was 500-fold lower compared with the frequency of incorporation of the correct nucleotide (dCMP) (Table 2). Overall, our steady-state kinetic data were indicative of low efficiency, high fidelity nucleotide insertion opposite the 10-mer peptide cross-linked to 7-deaza-G in DNA.

Sequence Analysis of Primer Extension Products by Liquid Chromatography-Tandem Mass Spectrometry—A mass spectrometry-based strategy reported previously (33–36) was used to sequence primer extension products of the translesion synthesis past peptide-dG conjugates. This method allows for detection of insertion, deletion, and point mutation products at the site of damage as well as any postlesion synthesis errors (34). Primer extension reactions were carried out with DNA duplexes containing native dG or the 10-mer peptide cross-link in the template strand (Fig. 3*D*). A uracil base was incorporated 3 nucleotides upstream from the primer end. Streptavidin capture of biotinylated primer extension products and treatment with UDG and hot piperidine allow for the release of short

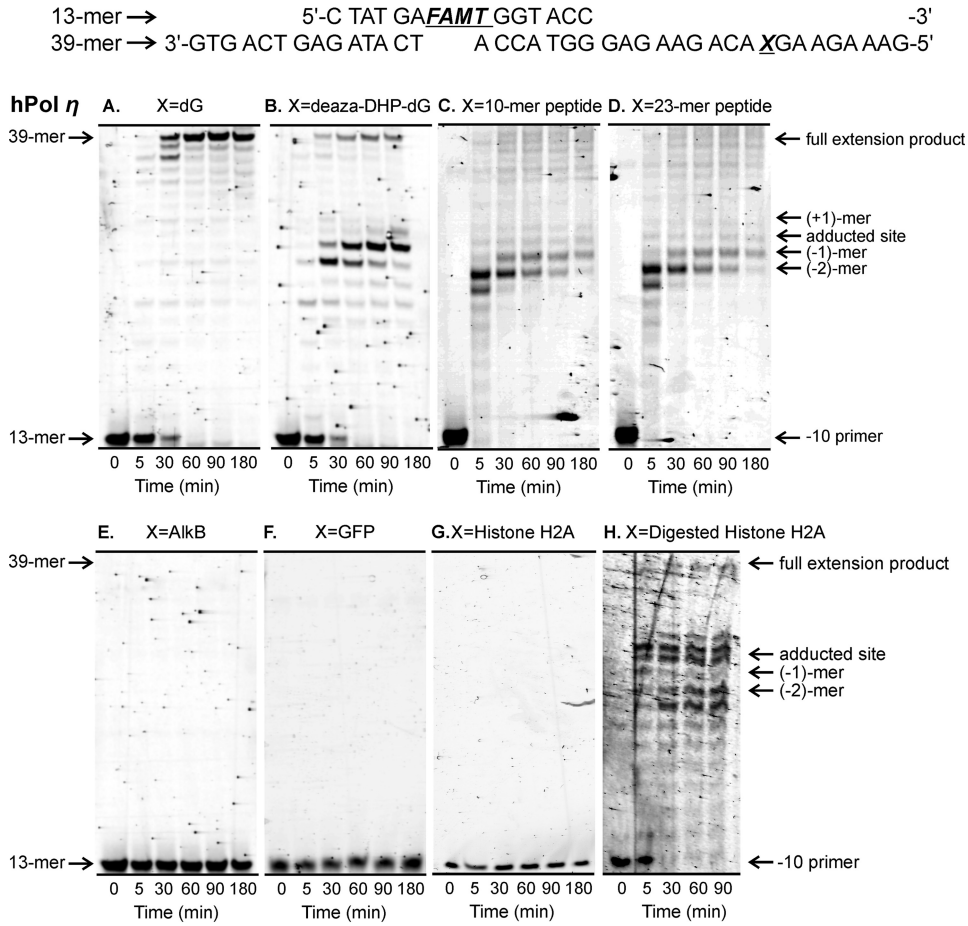

FIGURE 6. **Running start assays for replication bypass of DNA-protein cross-links by hPol η.** 13-mer FAMdT primers were annealed with 39-mers containing unmodified dG (*A*), deaza-DHP-dG (*B*), or covalent cross-links to 10-mer peptide EQKLISEEDL (*C*), 23-mer peptide PDAQLVPGINGKAIHLVNNESSE (*D*), or full-sized protein AlkB (*E*), histone H2A (*F*), or eGFP (*G*). The resulting primer-template complexes (0.15 μM) were incubated in the presence of hPol η (0.30 μM). Reactions were initiated by the addition of the four dNTPs (500 μM) and quenched at the indicated time points. Extension products were separated by 20% denaturing PAGE and visualized by fluorescence imaging. *Panel H* shows results for DPC to histone H2A following digestion with Proteinase K.

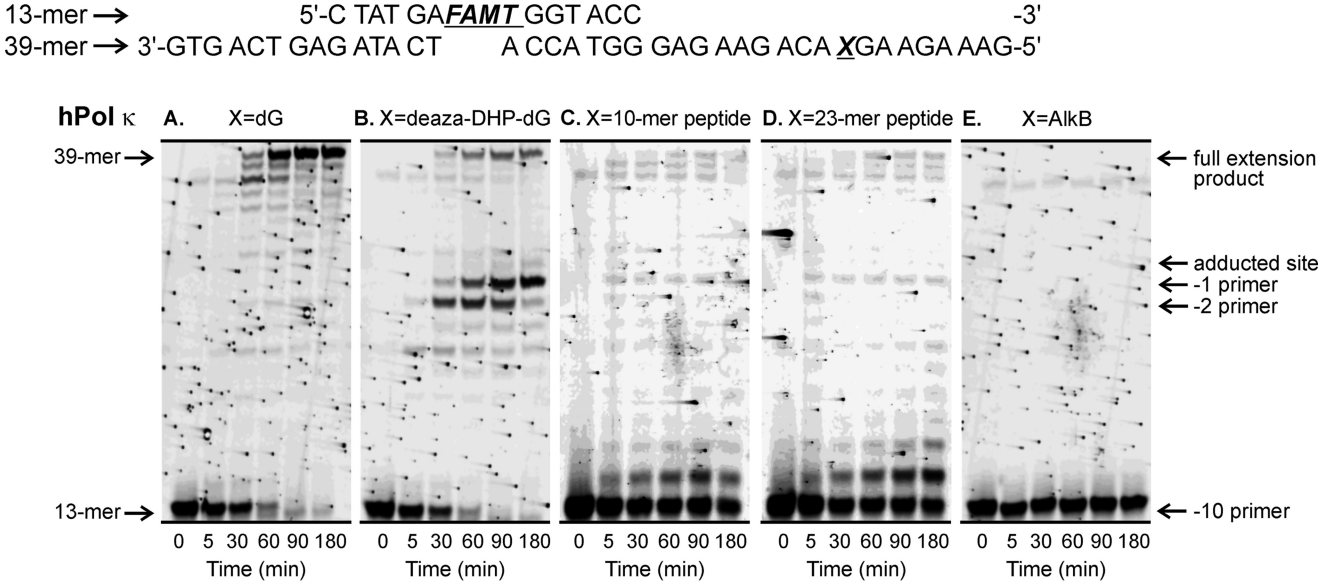

FIGURE 7. **Running start assays for replication bypass of DNA-peptide and DNA-protein cross-links by hPol κ.** 13-mer FAMdT primers were annealed with 39-mers containing unmodified dG (*A*), deaza-DHP-dG (*B*), or covalent cross-links to 10-mer peptide (*C*), 23-mer peptide (*D*), or AlkB protein (*E*). The resulting primer-template complexes (0.15 μM) were incubated in the presence of hPol κ (0.30 μM). Reactions were initiated by the addition of the four dNTPs (500 μM) and quenched at the indicated time points. Extension products were separated by 20% denaturing PAGE and visualized by fluorescence imaging.

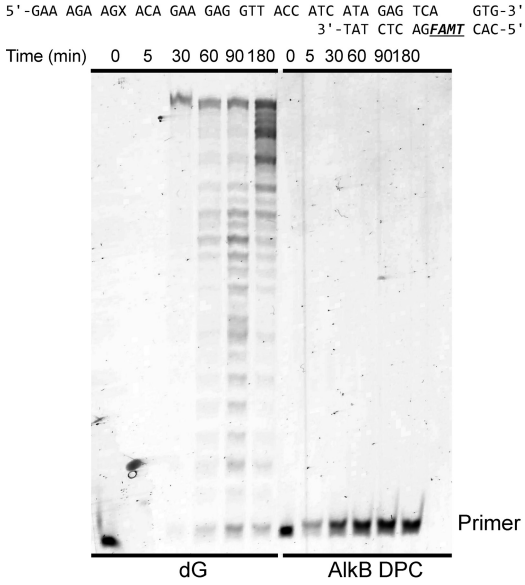

FIGURE 8. **Running start assays for replication bypass of DNA-peptide and DNA-protein cross-links by hPol η.** 12-mer FAMdT primers were annealed with 39-mers containing unmodified dG (negative control) or AlkB-DNA cross-link. The resulting primer-template complexes (0.15 μM) were incubated in the presence of hPol η (0.30 μM). Reactions were initiated by the addition of the four dNTPs (500 μM) and quenched at the indicated time points. Extension products were separated by 20% denaturing PAGE and visualized by fluorescence imaging.

oligodeoxynucleotide products containing the region of interest that are amenable for sequencing by HPLC-ESI-MS/MS (Fig. 12).

The extension products from hPol η-catalyzed primer extension reactions were sequenced by HPLC-ESI-FTMS/MS using an Orbitrap Velos mass spectrometer. The samples were initially analyzed in the full scan mode to detect all extension products. HPLC-ESI$^-$-FTMS peak areas in the extracted ion chromatograms corresponding to each product were compared with that of an internal standard to determine the relative quantities of each extension product.

Capillary HPLC-ESI$^-$-FTMS analysis of *in vitro* replication products resulting from primer extension reactions of template T4 containing 10-mer dG-peptide conjugate revealed one main peak corresponding to the accurate replication product (m/z 1002.16, $[M - 4H]^{4-}$). The MS/MS spectrum of this oligomer was consistent with the theoretical sequence (5′-pTG ***C***TA CCA GTG AC-3′; Fig. 12). Targeted HPLC-ESI$^-$-FTMS analyses failed to detect any point mutations, single nucleotide deletions, or postlesion synthesis errors. Taken together, our HPLC-ESI$^-$-FTMS/MS sequencing results are in agreement with the data from steady-state kinetic experiments (Table 2), indicating that nucleotide insertion opposite the 10-mer peptide conjugate by hPol η is largely accurate.

Modeling and Simulation—To better understand how the 10-mer peptide cross-link can be accommodated in the active site of TLS polymerases and copied with high fidelity, molecular dynamics simulations were carried out using a model for hPol κ developed earlier (37) based on the crystal structure of the hPol κ ternary complex by Lone *et al.* (38). The C7 atom of 7-deazaguanine is located in the DNA major groove. Modeling of the Ac-EQKLISEEDL-NH_2 cross-link was achieved by extending the longer N-terminal end of the peptide toward the 3′-end of the replicating DNA template (Fig. 13*A* and supplemental movie). Inspection of the trajectory showed an average Cα RMSD of 1.9 Å over the course of the 100-ns MD simulation, suggesting that the presence of the 10-mer cross-link within the major groove does not significantly affect the overall structure of hPol κ (Fig. 13*B*). The largest Cα RMSF of 3.6 Å occurred at Lys-204 in a turn of the palm region more than 30 Å away from the active site (Fig. 13*C*). All the interatomic distances between the incoming dCTP and the two Mg^{2+} ions were found to be conserved in the final structure of the simulation. The three Watson-Crick hydrogen bonds between 7-deazaguanine and the dCTP were present throughout the simulation, which would allow hPol κ to catalyze high fidelity nucleotide addition opposite the DNA-peptide lesion. However, the simulation also revealed that the Watson-Crick pairing was distorted because of the rigidity imposed on the damaged base by the cross-link and that there was steric crowding between the peptide lesion and the N-clasp domain of hPol κ (Fig. 13*A* and supplemental movie). This may contribute to inefficient lesion bypass and polymerase stalling at the peptide cross-link (Figs. 6 and 7).

Discussion

Lesion bypass is an important mechanism of cellular DNA damage tolerance as it allows for DNA replication past bulky nucleobase adducts that block DNA polymerases (39–43). Specialized TLS polymerases can be recruited to blocked replication forks and insert nucleotides opposite damaged bases (39–41, 43–49). TLS polymerases are catalytically less efficient than replicative enzymes and are much more error-prone because of their open and flexible active sites that accommodate large DNA adducts (43, 49–51) and their lack of intrinsic 3′ → 5′ proofreading activity (41, 46, 52–55). In humans, TLS polymerases include Y family polymerases hPols η, κ, and ι and Rev1, A family Pol ν, and B family Pol ζ (41, 43–49). Polymerase switching is thought to be regulated, at least in part, by posttranslational modifications of the proliferating cell nuclear antigen sliding clamp, which acts as a scaffold for polymerase enzymes (41, 43–49).

DPCs represent a special challenge to DNA replication because of their large size and their ability to distort DNA structure. DPCs had been hypothesized to completely block DNA polymerases, leading to stalling of replication forks (43, 56). In our earlier study, we found that model DPCs generated by copper-catalyzed [3 + 2] Huisgen cycloaddition (click reaction) between an alkyne group from 5-(octa-1,7-diynyl)-uracil in DNA and an azide group within engineered proteins/polypeptides completely blocked DNA replication, whereas the corresponding 10-mer peptide conjugate was bypassed in an error-prone manner (29, 36). In these model DPCs, peptides were conjugated to the C5 position of thymidine via a six-carbon linker (29). However, the majority of DNA-protein conjugates induced by antitumor nitrogen mustards such as mechlorethamine and chlorambucil, platinum compounds, dibromoethane, and diepoxides such as 1,2,3,4-diepoxybutane involve the N7 atom of G residues in DNA (3–5, 8, 10, 57), and the cross-

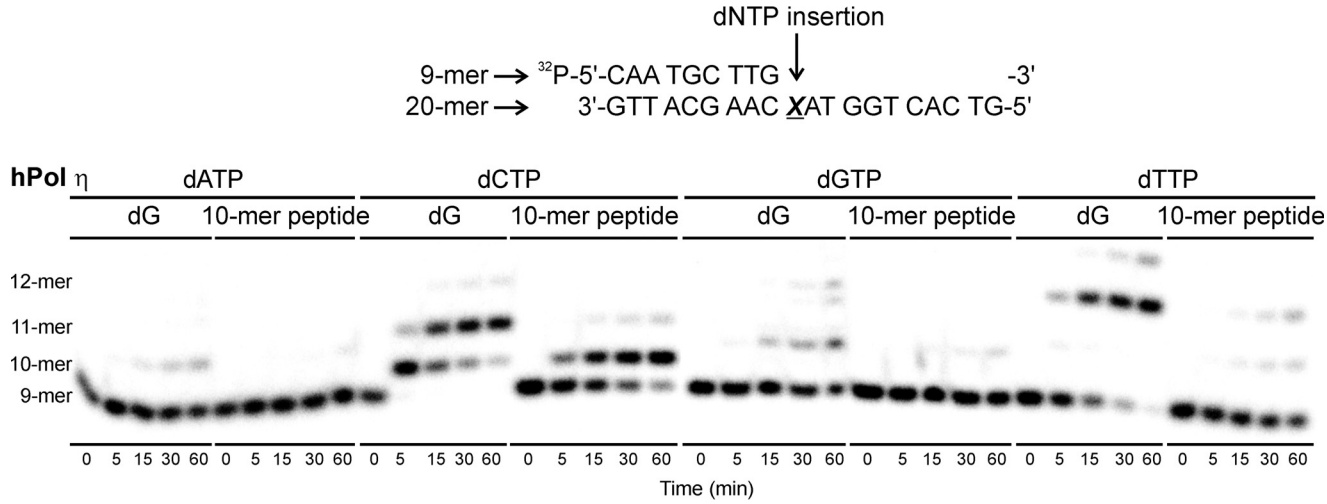

FIGURE 9. **Single nucleotide insertion opposite unmodified guanine (dG) and the 10-mer peptide cross-linked to C7 of 7-deazaguanine (10-mer peptide) by TLS polymerase hPol η.** Primer-template duplexes (50 nM) were incubated with 50 nM polymerase in the presence of 100 μM individual dNTPs. The reactions were quenched at predetermined time points (0–60 min), and the products were separated by 20% denaturing PAGE and visualized by phosphorimaging.

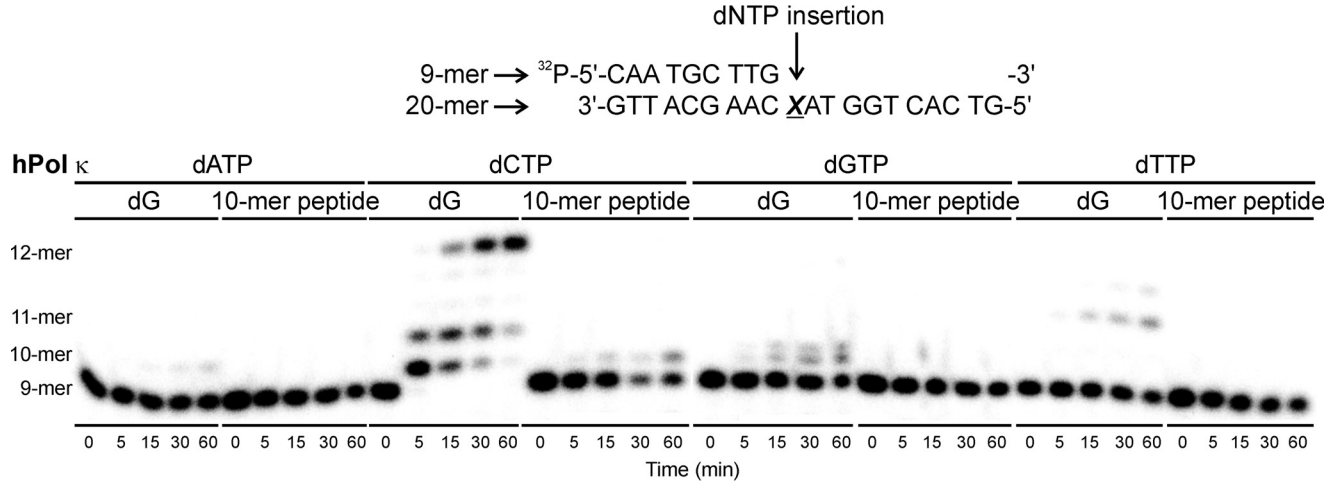

FIGURE 10. **Single nucleotide insertion opposite unmodified guanine (dG) and the 10-mer peptide cross-linked to C7 of 7-deazaguanine (10-mer peptide) by TLS polymerase hPol κ.** 50 nM primer-template duplexes were incubated with 150 nM polymerase in the presence 100 μM individual dNTPs. The reactions were quenched at predetermined time points (0–60 min), and the products were separated by 20% denaturing PAGE and visualized by phosphorimaging.

linking site within DNA duplex is likely to modulate the effects of DPC lesions on DNA replication.

*N*7-Guanine-conjugated DPCs are induced by many DNA cross-linking drugs such as nitrogen mustards, haloethylnitrosoureas, and platinum antitumor agents commonly used in the clinic to treat leukemia; lymphoma; ovarian adenocarcinoma; and breast, lung, and testicular cancers (58–62). The majority of *N*7-G lesions are labile to hydrolysis (23), making it difficult to synthesize site-specific DNA substrates containing such adducts for polymerase bypass assays. We recently developed a reductive amination methodology to prepare hydrolytically stable model 7-deaza-G DPC substrates that resemble DPCs formed by nitrogen mustards and dibromoethane (25). In the present study, this new methodology was used to prepare DNA-peptide and DNA-protein substrates of increasing size (1.3–28 kDa; Fig. 1). The resulting template-primer complexes were subjected to steady-state kinetics and polymerization experiments to investigate replication bypass of these bulky lesions by human TLS polymerases η and κ.

We found that human TLS polymerases η and κ were completely blocked by full size DPCs conjugated to the 7-deazaguanine within DNA (histone H4, 11.5 kDa; histone H2A, 14 kDa, AlkB, 23 kDa, and eGFP, 28 kDa) but were able to bypass the corresponding small peptide lesions (Figs. 4–7). DPC-induced replication blocks were observed in both standing start and running start experiments but were removed when the protein component of DPCs was digested with proteinase K (Figs. 4*H* and 6*H*). Importantly, the presence of DPC lesions affects polymerization at least 18 nucleotides upstream from the lesion, probably by interfering with polymerase loading (Fig. 8). These results are in agreement with our earlier primer extension studies of DPCs conjugated to the C5 position of thymidine (29). In both cases, the presence of TLS polymerases cannot overcome the replication block imposed by bulky protein-DNA conjugates. It should be noted that the C7 of G and the C5 of T occupy similar positions in the major groove of DNA.

Primer extension results shown here are consistent with published reports of polymerase blockage by DPCs *in vivo* (56,

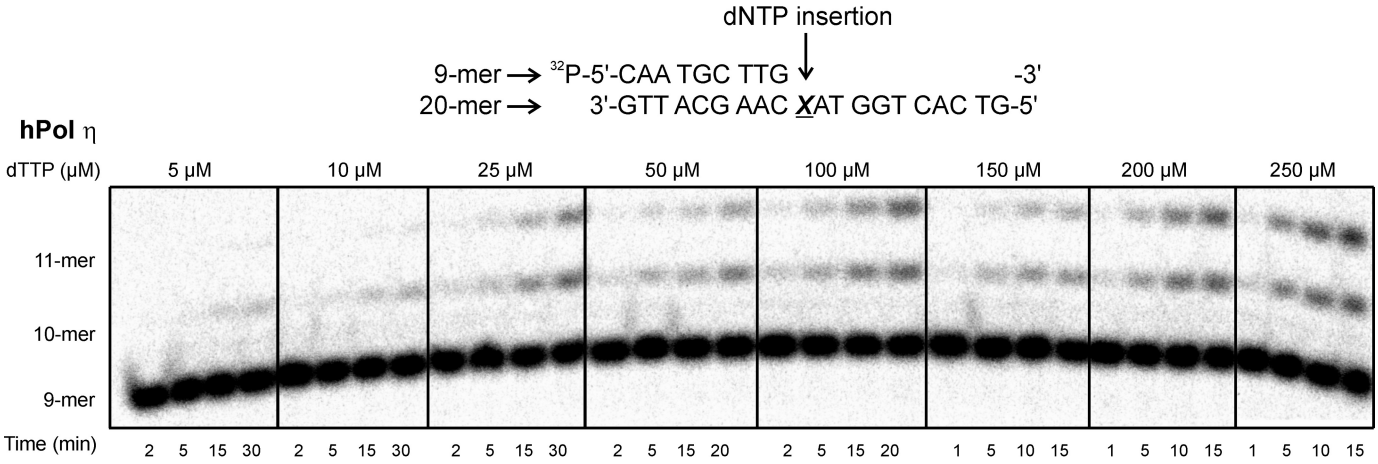

FIGURE 11. **Example of a steady-state kinetics experiment to determine the kinetics of single nucleotide insertion opposite the 10-mer peptide cross-linked to C7 of 7-deaza-G.** Single nucleotide incorporation assays were performed using hPol η and 10-mer peptide-deaza-G cross-links in the presence of increasing concentrations of individual dTTPs. Polymerization reactions were quenched at preselected time points and loaded onto 20% (w/v) denaturing polyacrylamide gels.

TABLE 2

Steady-state kinetic parameters for single nucleotide insertion opposite native dG (negative control) and the 10-mer peptide cross-linked to C7 of 7-deaza-G (10-mer peptide) by human TLS polymerases hPols κ and η

f, misinsertion frequency = $(k_{cat}/K_m)_{incorrect\ dNTP}/(k_{cat}/K_m)_{correct\ dNTP}$.

Polymerase	Template	Incoming nucleotide	k_{cat}	K_m	k_{cat}/K_m	*f*
			min^{-1}	μM	$\mu M^{-1}\ min^{-1}$	
hPol η	dG	dCTP	3.7 ± 0.2	2.6 ± 1.0	1.5	1
		dTTP	0.70 ± 0.08	120 ± 38	0.006	0.004
	10-mer peptide	dCTP	0.38 ± 0.04	13 ± 5	0.03	1
		dTTP	0.01 ± 0.001	32 ± 11	0.00005	0.002
hPol κ	dG	dCTP	0.53 ± 0.04	1.5 ± 1.1	0.37	1
	10-mer peptide	dCTP	0.02 ± 0.004	63 ± 24	0.0002	1

63, 64). For example, Kreuzer and co-workers (56) detected bubble and Y molecule accumulation in wild-type pBR322 plasmids containing methyltransferase (53.5 kDa) cross-linked to 5-azacytosine in *Escherichia coli*. Nakano *et al.* (63) found that the transformation efficiency of pGL3-CMV plasmids containing formaldehyde-induced cross-link to histone H1 (21.7 kDa) was <10% as compared with undamaged plasmid. In another study, the relative transformation efficiency of pMS2 plasmids containing UV-induced T4-pyrimidine dimer glycosylase (16 kDa) DPCs was found to be <5%, whereas that of UV-irradiated plasmids was ~50% (64). These results suggest that DPCs significantly hinder DNA replication *in vivo*.

In living cells, the protein component of DPC lesions may undergo proteolytic cleavage to smaller DNA-peptide or DNA-amino acid adducts, which represent a lesser block to polymerase bypass (65–68). For example, yeast Wss1 protease cleaves the protein constituent of DPC at blocked replisomes (21). Furthermore, repair of a plasmid-embedded DPC in *Xenopus* egg extracts is coupled to DNA replication (22). We found that the DPC-induced replication block is removed if the protein constituent of DPC is digested to amino acids with proteinase K (Figs. 4*H* and 6*H*). This is consistent with an earlier observation by Nakano *et al.* (63) that the transformation efficiency of pGL3-CMV plasmids containing partially digested histone H1 DPCs increased to 58% from <10% for plasmids containing undigested DPC.

To examine the influence of 7-deaza-G DNA-peptide lesions on replication efficiency and accuracy, we investigated primer extension past 10-mer and 23-mer peptides (EQKLISEEDL and PDAQLVPINGKAIHLVNNESSE) conjugated to a 7-deaza-G in an oligonucleotide. We found that both peptide conjugates were bypassed under running start conditions (Figs. 6, *C* and *D*, and 7, *C* and *D*), although the 23-mer peptide cross-link blocked replication in standing start experiments (see Figs. 4, *C* and *D*, and 5, *C* and *D*). Polymerase pause sites were observed 1–3 nucleotides prior to the adducted site (Fig. 6, *C* and *D*). Furthermore, both nucleotide insertion opposite DPC and postlesion synthesis were extremely inefficient (Figs. 6 and 7).

To our knowledge, this is the first investigation of the effects of 7-guanine-conjugated peptides on DNA replication in the presence of TLS polymerases. Previous studies have shown that Pol ν was able to catalyze primer extension past tetrapeptides and dodecapeptides cross-linked to the N^6 position of adenine (69), whereas the same peptides conjugated to the N^2-guanine position were bypassed by hPol κ and *E. coli* Pol IV (70). In our earlier study, the same 10-mer peptide conjugated to C5 of thymine via a six-carbon linker was bypassed by hPol κ and hPol η (29). Taken together, these results indicate that unlike DPCs containing full size proteins peptide conjugates can be tolerated by human TLS polymerases.

Steady-state kinetic experiments have revealed that the efficiencies of dCMP insertion opposite 7-deaza-G DNA-peptide

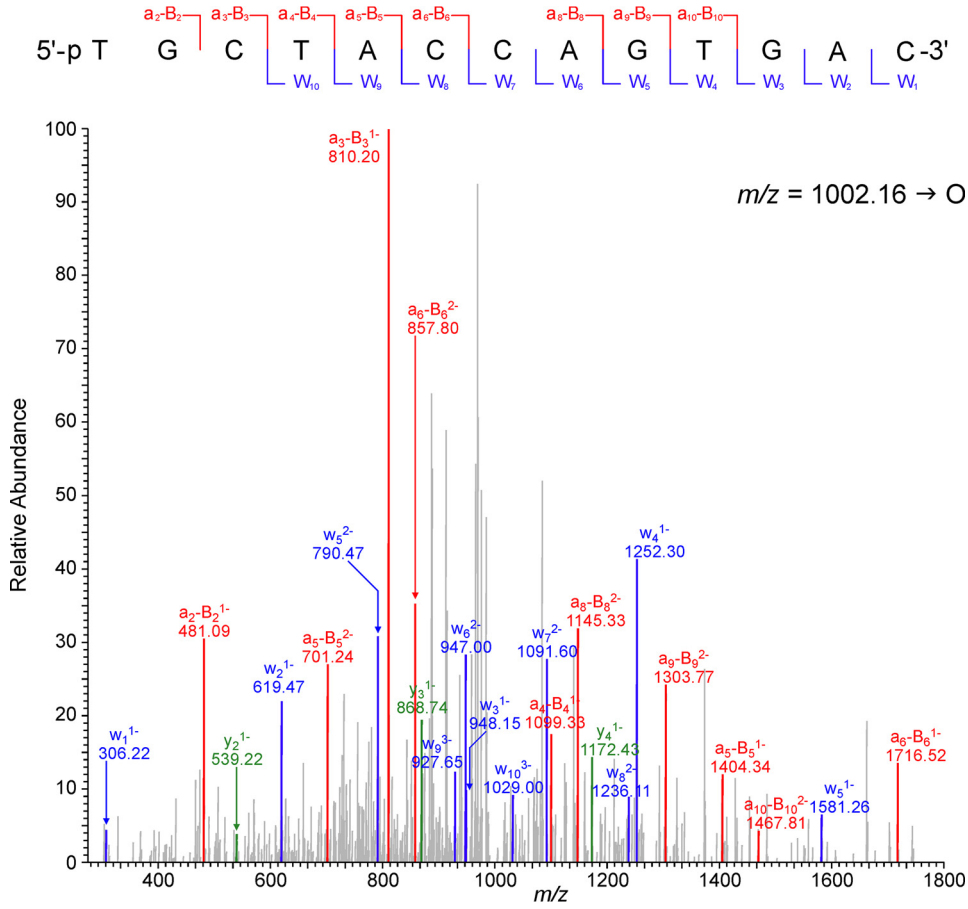

FIGURE 12. **Collision-induced dissociation mass spectra of the error-free extension products observed following hPol η-catalyzed replication past the 10-mer peptide cross-linked to 7-deazaguanine.**

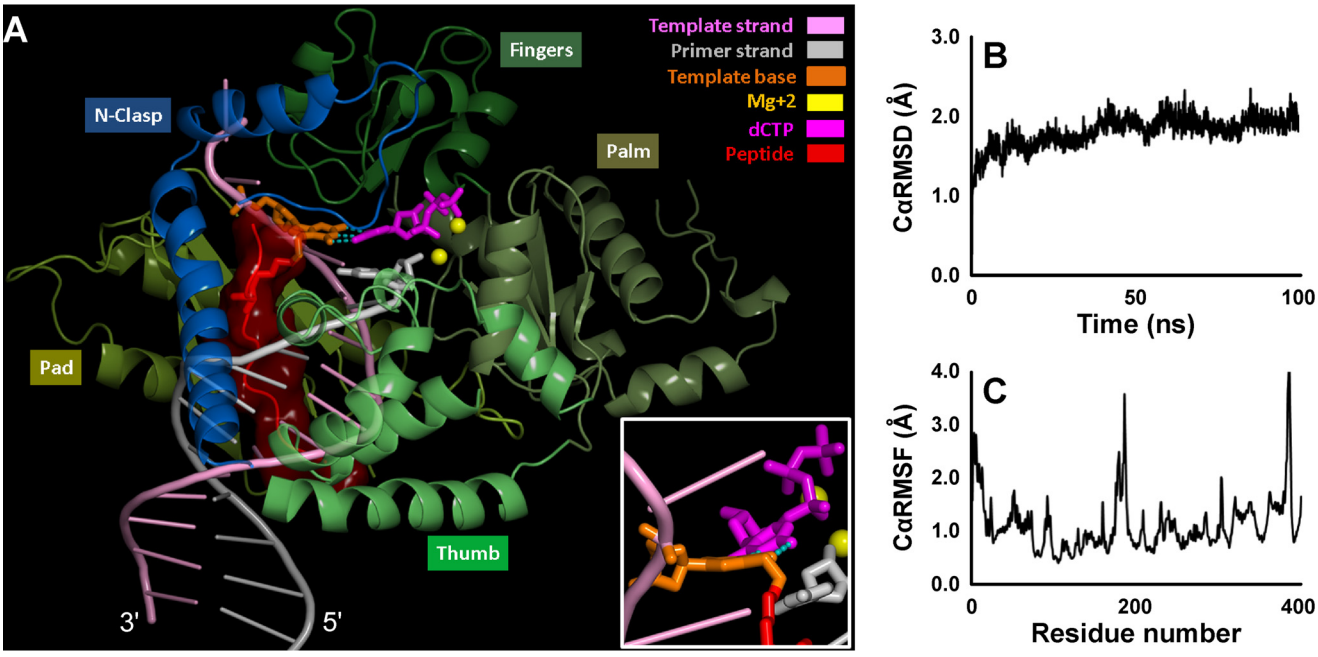

FIGURE 13. *A*, MD snapshot at 100 ns of the hPol κ-DNA ternary complex containing the 10-mer peptide cross-linked to 7-deazaguanine. The complex is displayed in schematic mode except for the dCTP and the cross-link-containing template base, which are in *stick*. The peptide is shown in *red surface*. The three Watson-Crick hydrogen bonds are shown with *dotted lines*. The *inset*, rotated about 90° along the *y* axis, highlights the Watson-Crick pair distortion. A rotating view is given in the supplemental movie. Cα RMSD (*B*) and Cα RMSF (*C*) of the hPol κ over the course of the 100-ns MD simulation for the hPol κ-DNA ternary complex containing the lesion peptide.

conjugates by hPol η and hPol κ were 49- and 1850-fold lower than for the template containing native G (Table 2). As observed previously for *C*5-thymine lesions (36), hPol η was more efficient than hPol κ. Higher catalytic efficiency of hPol η than hPol κ is consistent with previous reports for other bulky nucleobase lesions such as exocyclic adducts (35, 71–73) and DNA-glutathione conjugates (74).

Unlike *C*5-thymine-peptide lesions, which induce high numbers of frameshift and base substitution mutations upon primer extension in the presence of hPol κ and hPol η (36), *C*7-G conjugated DPCs were not miscoding. Our gel electrophoresis and mass spectrometry experiments have shown that replication bypass of the 10-mer peptide cross-linked to *C*7-G by hPol κ was essentially error-free, whereas hPol η incorporated the correct base (dC) with 500-fold preference over the mispair (dT) (Table 2 and Figs. 9 and 10). These results indicate that the biological outcomes of DNA-peptide lesions are largely defined by the cross-linking site on DNA (C7 of deazaguanine *versus* C5 of thymine).

Our model cross-links differ from lesions formed in cells by the absence of a positive charge on the guanine 7-position. The replacement of *N*7-guanine with carbon introduces changes in hydration and charge localization (75). However, 7-deazaguanine-containing DNA has essentially the same structure as native DNA (76), and 7-deazaguanine mimics have been successfully used in a number of previous studies of DNA lesion repair and polymerase bypass (27, 77–79).

Molecular dynamics simulations based on the published crystal structure of a hPol κ-DNA template-primer-dCTP ternary complex (37, 38) indicated that the 10-mer peptide conjugated to 7-deaza-G can be accommodated in the major groove of the DNA oriented toward the 3′-end of the template strand with minimal overall structural perturbations (Cα RMSD of 1.9 Å; Fig. 13*B*). The Watson-Crick base pairing between the 7-deazaguanine and the incoming dCTP explains the observed high fidelity bypass results (Table 2). However, the rigidity imposed on the damaged base by the cross-link causes the Watson-Crick base pair to be distorted, which explains the reduced nucleotide incorporation efficiency. Furthermore, the close contact of the peptide with the hPol κ N-clasp likely causes polymerase stalling by hindering translocation, which is expected to impede extension efficiency and hinder postlesion synthesis (Fig. 13*A* and supplemental movie). Other bulky major groove DNA lesions are also known to stall hPol κ (80, 81).

hPol η and hPol κ have very significant structural differences (82). One important difference in relation to our experimental results is the absence of the N-clasp in hPol η. Consequently, the DNA major groove of the primer-template complex with hPol η remains open, allowing for ready accommodation of the 7-deazaguanine 10-mer peptide cross-link. The cross-linked template is expected to retain Watson-Crick pairing at the 5′-templating base but distort the pairing and impede translocation due to the rigidity of the damaged base. Thus, the greater efficiency and fidelity of hPol η compared with hPol κ very likely stems from the absence of the N-clasp, whereas the overall high fidelity but low efficiency in the two polymerases has a common origin in the lesion structure.

In summary, we have examined the ability of human lesion bypass polymerases to catalyze replication past DNA-protein and DNA-peptide cross-links conjugated to the major groove of DNA via the C7 atom of deazaguanine. We found that large DNA-protein and DNA-peptide cross-links completely blocked human TLS polymerases, whereas smaller peptide cross-links were bypassed with low efficiency but with high fidelity. The 7-deazaguanine DNA substrates used here are structurally analogous to the major DNA-protein cross-links formed *in vivo* when cancer patients are treated with nitrogen mustard drugs (3). These results suggest that proteolytic degradation of toxic DPCs to smaller DNA-peptide cross-links allows for them to be bypassed in an accurate manner by human TLS polymerases.

Experimental Procedures

Materials—Fluorescein-dT phosphoramidite, protected 2′-deoxyribonucleoside 3′-phosphoramidites (dA-CE, Ac-dC-CE, dmf-dG-CE, and dT-CE), Ac-dC-CPG ABI, dmf-dG-CPG ABI columns, and all other reagents required for automated DNA synthesis were purchased from Glen Research (Sterling, VA). Recombinant human DNA polymerases hPols η and κ were expressed and purified as described elsewhere (84, 85). Recombinant AlkB protein was a generous donation from Prof. Chuan He (Department of Chemistry, University of Chicago). Expression of His_6-eGFP protein (referred to as eGFP throughout) (86) and synthesis of 23-mer and 10-mer peptides (PDAQLVPINGKAIHLVNNESSE and EQKLISEEDL) (29) were carried out according to previously reported protocols. T4 polynucleotide kinase (PNK) and recombinant histones H2A and H4 were obtained from New England Biolabs (Beverly, MA); [γ-^{32}P]ATP was purchased from PerkinElmer Life Sciences. 40% 19:1 acrylamide/bisacrylamide solution and Micro Bio-Spin 6 columns were purchased from Bio-Rad. Unlabeled dNTPs were obtained from Omega Bio-Tek (Norcross, GA). Size exclusion columns (NAP-5 and Microspin G25) and Sep-Pak C_{18} solid phase extraction cartridges were obtained from GE Healthcare and Waters (Milford, MA), respectively. All other chemicals and solvents were purchased from Sigma-Aldrich and were of the highest grade available.

Synthesis and Characterization of Oligodeoxynucleotides—Synthetic oligonucleotides containing site-specific 7-deaza-7-(2,3-dihydroxypropan-1-yl)-2′-deoxyguanosine (5′-G TCA CTG GTA ***deaza-DHP-dG***CA AGC ATT G-3′ and 5′-GAA AGA AG***deaza-DHP-dG*** ACA GAA GAG GGT ACC ATC ATA GAG TCA GTG-3′) were prepared as described previously (27). Primers internally labeled with 5′-[*N*-((fluoresceinyl)-aminohexyl)-3-acrylimido]-2′-deoxyuridine (5′-CAA ***FAMdT***GC TTG-3′ and 5′-CTA TGA ***FAMdT***GG TAC C-3′) and native DNA strands (5′-G TCA CTG GTA GCA AGC ATT G-3′, 5′-GAA AGA AGG ACA GAA GAG GGT ACC ATC ATA GAG TCA GTG-3′, and 5′-CAA TGC TTG-3′) were prepared by standard solid phase synthesis using an ABI 394 DNA synthesizer (Applied Biosystems, Foster City, CA). Biotinylated 19-mer primers (biotin-5′-T_{10} CAA TGC UTG-3′) were purchased from Integrated DNA Technologies (Coralville, IA). All synthetic oligodeoxynucleotides were purified by semiprepara-

tive HPLC, desalted by Illustra NAP-5 columns, and characterized by HPLC-ESI$^-$-MS.

Synthesis and Characterization of DNA-Protein and DNA-Peptide Cross-links—Site-specific DNA-protein and DNA-peptide cross-links were generated by a postsynthetic reductive amination strategy developed in our laboratory (25). Briefly, synthetic DNA oligomers containing site-specific deaza-DHP-dG (1 nmol in 36 μl of water) were oxidized in the presence of 50 mM $NaIO_4$ (70 μl) in 15 mM sodium phosphate buffer (pH 5.4; 70 μl) for 6 h at 4 °C in the dark to convert deaza-DHP-dG to 7-deaza-7-(2-oxoethyl)-2′-deoxyguanosine (Fig. 1). Excess $NaIO_4$ was quenched with Na_2SO_3 (55 mM; 70 μl), and the resulting aldehyde-functionalized DNA was incubated with the protein of interest (AlkB, histone H4, histone H2A, or eGFP; 2–10-fold molar excess) in the presence of 25 mM $NaCNBH_3$ at 37 °C overnight to generate DNA-protein cross-links (Fig. 1). The resulting DNA-protein conjugates (Table 1) were purified using 20% (w/v) denaturing polyacrylamide gels containing 7 M urea.

DNA-peptide conjugates were prepared analogously (Fig. 1) except that a 10–100-fold molar excess of the peptide was used, and the pH was adjusted to 7.0 prior to peptide addition. DNA-peptide conjugates were isolated using 20% (w/v) denaturing polyacrylamide gels containing 7 M urea. DNA-protein and DNA-peptide cross-links were desalted by Micro Bio-Spin 6 columns and Sep-Pak C_{18} solid phase extraction cartridges, respectively. The purified conjugates were characterized by HPLC-ESI$^+$-MS/MS as described previously (25). To assess DPC purity, aliquots of the purified samples were radiolabeled with γ-^{32}P and resolved on 20% (w/v) denaturing polyacrylamide gels containing 7 M urea followed by visualization using a Typhoon FLA 7000 phosphorimaging system (GE Healthcare). Depending on the purity of the cross-links obtained, additional gel purifications were carried out to achieve >98% purity.

Preparation of Primer-Template Duplexes—For primer extension assays, fluorescein-labeled primer P1 or P2 (Table 1; 50 pmol) were mixed with 2 eq of template strands containing dG (T1 or T10), deaza-DHP-dG (T2 or T11), or model DPCs (T3–T9 or T12–T16 in Table 1) in 10 mM Tris-HCl buffer (pH 8.0) containing 50 mM NaCl. The mixtures were heated at 95 °C for 10 min and allowed to cool overnight to afford the corresponding primer-template duplexes.

For steady-state experiments to determine the kinetics of single nucleotide insertion opposite the cross-links, the 9-mer 5′-CAA TGC TTG-3′ (1 nmol) was radiolabeled with T4 PNK (20 units) and [γ-^{32}P]ATP (25 μCi) in the presence of T4 PNK reaction buffer (total volume, 20 μl) at 37 °C for 1 h to obtain primer P3 (Table 1). The mixtures were heated at 65 °C for 10 min to inactivate the enzyme and passed through Illustra Microspin G25 columns to remove excess [γ-^{32}P]ATP. 5′-^{32}P-Labeled primer P3 (Table 1; 50 pmol) was annealed to template strands (5′-G TCA CTG GTA *X*CA AGC ATT G-3′) containing unmodified dG (T1 in Table 1) or 7-deaza-dG-10-mer peptide cross-link (T4 in Table 1). For HPLC-ESI$^-$-MS/MS sequencing of extension products, biotinylated primers P4 (Table 1; 100 pmol) were annealed to the template strands containing either unmodified dG or the dG-10-peptide conjugate at position *X* (T1 or T4 in Table 1; 200 pmol).

Primer Extension Assays—For standing start experiments, DNA complexes containing primer P1 annealed to templates T1–T9 in Table 1 (0.15 μM; Fig. 3*A*) were incubated with human DNA polymerase η or κ (0.30 μM) at room temperature in the presence of a buffered solution containing 50 mM Tris (pH 7.5), 50 mM NaCl, 5 mM DTT, 100 μg/ml BSA, 10% glycerol (v/v), and 5 mM $MgCl_2$. Polymerization reactions were initiated by adding a solution containing all four dNTPs (0.5 mM each). Aliquots of the reaction mixtures (4 μl) were withdrawn at preselected time intervals (0, 5, 30, 60, 90, and 180 min) and quenched by the addition of 95% (v/v) formamide containing 10 mM EDTA (18 μl). Samples were loaded onto 20% (w/v) denaturing polyacrylamide gels and run at 80 watts for 3 h. The extension products were visualized using a Typhoon FLA 7000 in the fluorescence imaging mode. Running start experiments were conducted in a similar manner using 13-mer FAMdT primer-39-mer template DNA duplexes (Fig. 3*B*).

Single Nucleotide Incorporation Assays—^{32}P-End-labeled primer-template duplexes containing native dG or 10-mer peptide-deaza-dG conjugate (50 nM) at position *X* (Fig. 3*C*) were incubated with human TLS polymerases (50 nM hPol η or 150 nM hPol κ) in 50 mM Tris-HCl (pH 7.5) buffer containing 50 mM NaCl, 5 mM DTT, 5 mM $MgCl_2$, 100 μg/ml BSA, and 10% (v/v) glycerol at room temperature. Polymerization reactions were initiated by the addition of individual dNTPs (100 μM) in a final volume of 20 μl. Aliquots (4 μl) were withdrawn at preselected time points, and the reactions were quenched by the addition of a solution containing 10 mM EDTA, 0.03% (w/v) bromphenol blue, and 0.03% (w/v) xylene cyanol in 95% (v/v) formamide (8 μl). The extension products were resolved by 20% (w/v) denaturing PAGE containing 7 M urea and visualized using a Typhoon FLA 7000 phosphorimaging system.

Steady-state Kinetic Analyses—The steady-state kinetics for incorporation of individual nucleotides opposite the native dG or the 10-mer peptide-deaza-dG cross-link were investigated by performing single nucleotide incorporation assays with 0.5–50 nM hPol η or 3–55 nM hPol κ in the presence of increasing concentrations of individual dNTPs (0–500 μM). Polymerization reactions were quenched at preselected time points (0–60 min). The product bands were visualized using a Typhoon FLA 7000 phosphorimaging system and quantified by volume analysis using Image Quant TL 8.0 software (GE Healthcare). Steady-state kinetic parameters were calculated by nonlinear regression analysis using one-site hyperbolic fits in Prism 4.0 (GraphPad Software, La Jolla, CA).

Sequencing of hPol η Primer Extension Products by Liquid Chromatography-Tandem Mass Spectrometry—Biotinylated primer-template duplexes (150 pmol) prepared by annealing uracil-containing primer P4 with template T1 or T4 (Table 1 and Fig. 3*D*) were incubated with hPol η (60 pmol) in 50 mM Tris-HCl (pH 7.5) buffer containing 50 mM NaCl, 5 mM DTT, 5 mM $MgCl_2$, 100 μg/ml BSA, and a 1 mM concentration each of the four dNTPs. Following a 6-h incubation at room temperature, biotinylated DNA strands were captured on streptavidin beads. Briefly, 20 mM sodium phosphate (pH 7.0) buffer containing 150 mM NaCl (400 μl) was added to each reaction. Streptavidin-Sepharose high performance beads (0.2 ml; GE Healthcare) were washed with 500 μl of 20 mM sodium phos-

phate (pH 7.0) buffer containing 150 mM NaCl and then added to the polymerase reaction mixture. The resulting suspension was incubated at room temperature for 2 h with mixing every 10 min. Following binding of the biotinylated DNA to the beads, the supernatant was removed, and the beads were washed three times with water (300 μl). A solution of 50 mM Tris-HCl buffer (pH 7.5) containing uracil-DNA glycosylase (20 units), 1 mM EDTA, and 1 mM DTT (500 μl) was added followed by incubation at 37 °C for 4 h. The beads were washed three times with H_2O (300 μl) and then incubated with 250 mM piperidine (400 μl) at 95 °C for 1 h to cleave the abasic sites resulting from uracil-DNA glycosylase-mediated excision of U. The resulting samples were dried *in vacuo*, and the residue was reconstituted in 25 μl of water containing a 14-mer internal standard (5′-pCTT CAC GAG CCC CC-3′; 40 pmol).

Capillary HPLC-ESI$^-$-MS/MS analyses were conducted as described previously (36). An Agilent 1100 HPLC system (Agilent Technologies, Wilmington, DE) coupled to a Thermo LTQ Orbitrap Velos mass spectrometer (Thermo Fisher Scientific, Waltham, MA) was operated in the negative ion ESI-FTMS/MS mode. HPLC separation was conducted using an Agilent Zorbax 300SB-C_{18} column (0.5 × 150 mm; 5 μm) eluted with a gradient of 15 mM $NH_4(CH_3CO_2)$ (buffer A) and CH_3CN (buffer B) at a flow rate of 15 μl/min. The percentage of solvent B was changed linearly from 1 to 10% in 24 min, further to 75% in 1 min, held at 75% for 3 min, and finally brought back to 1% in 2 min (all v/v). Nucleotide sequences of the extension products were confirmed by comparing the observed MS/MS fragments to the expected collision-induced dissociation fragmentation patterns of oligodeoxynucleotides (Mongo Oligo mass calculator version 2.06, available online from The RNA Institute, College of Arts and Sciences, State University of New York at Albany).

Modeling and Simulation—All molecular modeling was carried out using the Schrödinger modeling package (Schrödinger LLC, New York, NY). The starting model of hPol κ in complex with unmodified DNA was based on our earlier publication (37). We placed the Ac-EQKLISEEDL-NH_2 peptide lesion with its N terminus directed toward the 3′-end of the template strand; the opposite orientation, in the 5′-direction, is crowded, whereas the 3′-orientation places the peptide comfortably in the major groove. The templating G within the polymerase active site was replaced by a 7-deazaguanine and conjugated to the side chain of a single lysine residue via a two-carbon linker (Fig. 1). Individual amino acids were iteratively added and locally minimized with fixed protein backbone and DNA until the full sequence of the 10-mer peptide (Ac-QKLISEEDL-NH_2 where lysine is conjugated to DNA) was assembled. The final model was solvated with a 15-Å buffer region of explicit TIP3 water layer containing 0.15 M NaCl as counterions inside a rectangular box. The long range electrostatic interactions were evaluated by the particle mesh Ewald method under periodic boundary conditions. MD simulation was carried out using Desmond (D. E. Shaw Research, New York, NY) with the default initialization protocol followed by a 100-ns production simulation run under isothermal isobaric (NPT) conditions at 300 K and 1 atm with the OPLS-AA 2005 force field. A force constant of 50 kcal/mol Å^2 restraint was applied to the heavy atoms of DNA. The structural changes to hPol κ in the presence of the 10-mer peptide cross-link were assessed by evaluating the Cα RMSF and the Cα RMSD of the protein with respect to the minimized starting structure.

Author Contributions—N. T. conceived and directed the studies. Y. S. and M. G. P. prepared recombinant DNA polymerases. S. W. and S. J. conducted steady-state kinetics analyses and LC-MS analyses. S. M. and O. D. S. synthesized oligonucleotide containing deaza-DHP-dG. Y. Y. S. conducted molecular modeling. L. L.-H. and I. F. interpreted molecular modeling results and generated figures for publication. S. W. and N. T. wrote the paper with the help of Y. Y. S., M. D., S. B., O. D. S., and F. P. G.

Acknowledgments—We thank Dr. Chuan He (Department of Chemistry, University of Chicago) for the generous donation of recombinant AlkB protein, Dr. Dan Harki and Dr. Angela Perkins (Department of Medicinal Chemistry, University of Minnesota) for synthesizing the Ac-Myc peptide, Jeffrey Vervacke for synthesizing the tetanus toxoid peptide, and Bob Carlson (Masonic Cancer Center, University of Minnesota) for preparing the figures for this manuscript. We thank the University of Minnesota Supercomputing Institute for providing all the necessary computational resources.

References

1. Barker, S., Weinfeld, M., and Murray, D. (2005) DNA-protein crosslinks: their induction, repair, and biological consequences. *Mutat. Res.* **589,** 111–135
2. Ide, H., Shoulkamy, M. I., Nakano, T., Miyamoto-Matsubara, M., and Salem, A. M. (2011) Repair and biochemical effects of DNA-protein cross-links. *Mutat. Res.* **711,** 113–122
3. Loeber, R. L., Michaelson-Richie, E. D., Codreanu, S. G., Liebler, D. C., Campbell, C. R., and Tretyakova, N. Y. (2009) Proteomic analysis of DNA-protein cross-linking by antitumor nitrogen mustards. *Chem. Res. Toxicol.* **22,** 1151–1162
4. Michaelson-Richie, E. D., Ming, X., Codreanu, S. G., Loeber, R. L., Liebler, D. C., Campbell, C., and Tretyakova, N. Y. (2011) Mechlorethamine-induced DNA-protein cross-linking in human fibrosarcoma (HT1080) cells. *J. Proteome. Res.* **10,** 2785–2796
5. Michaelson-Richie, E. D., Loeber, R. L., Codreanu, S. G., Ming, X., Liebler, D. C., Campbell, C., and Tretyakova, N. Y. (2010) DNA-protein cross-linking by 1,2,3,4-diepoxybutane. *J. Proteome Res.* **9,** 4356–4367
6. Barker, S., Weinfeld, M., Zheng, J., Li, L., and Murray, D. (2005) Identification of mammalian proteins cross-linked to DNA by ionizing radiation. *J. Biol. Chem.* **280,** 33826–33838
7. Tretyakova, N. Y., Groehler, A., 4th, and Ji, S. (2015) DNA-protein cross-links: formation, structural identities, and biological outcomes. *Acc. Chem. Res.* **48,** 1631–1644
8. Ming, X. (2011) *DNA-Protein Cross-linking by cis-1,1,2,2-Diamminedichloroplatinum(II) (Cisplatin)*. M.Sc. thesis, University of Minnesota
9. O'Connor, P. M., and Fox, B. W. (1989) Isolation and characterization of proteins cross-linked to DNA by the antitumor agent methylene dimethanesulfonate and its hydrolytic product formaldehyde. *J. Biol. Chem.* **264,** 6391–6397
10. Gherezghiher, T. B., Ming, X., Villalta, P. W., Campbell, C., and Tretyakova, N. Y. (2013) 1,2,3,4-Diepoxybutane-induced DNA-protein cross-linking in human fibrosarcoma (HT1080) cells. *J. Proteome Res.* **12,** 2151–2164
11. Bau, D. T., Wang, T. S., Chung, C. H., Wang, A. S., Wang, A.S., and Jan, K. Y. (2002) Oxidative DNA adducts and DNA-protein cross-links are the major DNA lesions induced by arsenite. *Environ. Health Perspect.* **110,** 753–756

12. Zhitkovich, A., Voitkun, V., Kluz, T., and Costa, M. (1998) Utilization of DNA-protein cross-links as a biomarker of chromium exposure. *Environ. Health Perspect.* **106,** 969–974
13. Chakrabarti, S. K., Bai, C., and Subramanian, K. S. (1999) DNA-protein crosslinks induced by nickel compounds in isolated rat renal cortical cells and its antagonism by specific amino acids and magnesium ion. *Toxicol. Appl. Pharmacol.* **154,** 245–255
14. Nakano, T., Terato, H., Asagoshi, K., Masaoka, A., Mukuta, M., Ohyama, Y., Suzuki, T., Makino, K., and Ide, H. (2003) DNA-protein cross-link formation mediated by oxanine. A novel genotoxic mechanism of nitric oxide-induced DNA damage. *J. Biol. Chem.* **278,** 25264–25272
15. Dizdaroglu, M., and Gajewski, E. (1989) Structure and mechanism of hydroxyl radical-induced formation of a DNA-protein cross-link involving thymine and lysine in nucleohistone. *Cancer Res.* **49,** 3463–3467
16. Gajewski, E., and Dizdaroglu, M. (1990) Hydroxyl radical induced cross-linking of cytosine and tyrosine in nucleohistone. *Biochemistry* **29,** 977–980
17. Gueranger, Q., Kia, A., Frith, D., and Karran, P. (2011) Crosslinking of DNA repair and replication proteins to DNA in cells treated with 6-thioguanine and UVA. *Nucleic Acids Res.* **39,** 5057–5066
18. Tretyakova, N. Y., Michaelson-Richie, E. D., Gherezghiher, T. B., Kurtz, J., Ming, X., Wickramaratne, S., Campion, M., Kanugula, S., Pegg, A. E., and Campbell, C. (2013) DNA-reactive protein monoepoxides induce cell death and mutagenesis in mammalian cells. *Biochemistry* **52,** 3171–3181
19. Groehler, A., 4th, Villalta, P. W., Campbell, C., and Tretyakova, N. (2016) Covalent DNA-protein cross-linking by phosphoramide mustard and nornitrogen mustard in human cells. *Chem. Res. Toxicol.* **29,** 190–202
20. Stingele, J., Schwarz, M. S., Bloemeke, N., Wolf, P. G., and Jentsch, S. (2014) A DNA-dependent protease involved in DNA-protein crosslink repair. *Cell* **158,** 327–338
21. Stingele, J., Habermann, B., and Jentsch, S. (2015) DNA-protein crosslink repair: proteases as DNA repair enzymes. *Trends Biochem. Sci.* **40,** 67–71
22. Duxin, J. P., Dewar, J. M., Yardimci, H., and Walter, J. C. (2014) Repair of a DNA-protein crosslink by replication-coupled proteolysis. *Cell* **159,** 346–357
23. Singer, B., and Grunberger, D. (1983) *Molecular Biology of Mutagens and Carcinogens*, Plenum Press, New York
24. Gates, K. S., Nooner, T., and Dutta, S. (2004) Biologically relevant chemical reactions of N7-alkylguanine residues in DNA. *Chem. Res. Toxicol.* **17,** 839–856
25. Wickramaratne, S., Mukherjee, S., Villalta, P. W., Schärer, O. D., and Tretyakova, N. Y. (2013) Synthesis of sequence-specific DNA-protein conjugates via a reductive amination strategy. *Bioconjug. Chem.* **24,** 1496–1506
26. Loecken, E. M., and Guengerich, F. P. (2008) Reactions of glyceraldehyde 3-phosphate dehydrogenase sulfhydryl groups with bis-electrophiles produce DNA-protein cross-links but not mutations. *Chem. Res. Toxicol.* **21,** 453–458
27. Angelov, T., Guainazzi, A., and Schärer, O. D. (2009) Generation of DNA interstrand cross-links by post-synthetic reductive amination. *Org. Lett.* **11,** 661–664
28. Ho, T. V., Guainazzi, A., Derkunt, S. B., Enoiu, M., and Schärer, O. D. (2011) Structure-dependent bypass of DNA interstrand crosslinks by translesion synthesis polymerases. *Nucleic Acids Res.* **39,** 7455–7464
29. Yeo, J. E., Wickramaratne, S., Khatwani, S., Wang, Y. C., Vervacke, J. , Distefano, M. D., and Tretyakova, N. Y. (2014) Synthesis of site-specific DNA-protein conjugates and their effects on DNA replication. *ACS Chem. Biol.* **9,** 1860–1868
30. Nilsson, J. A., and Cleveland, J. L. (2003) Myc pathways provoking cell suicide and cancer. *Oncogene* **22,** 9007–9021
31. Hoffman, B., and Liebermann, D. A. (2008) Apoptotic signaling by c-MYC. *Oncogene* **27,** 6462–6472
32. Geacintov, N. E., and Broyde, S. (2010) *The Chemical Biology of DNA Damage*, Wiley, Hoboken, NJ
33. Zang, H., Goodenough, A. K., Choi, J. Y., Irimia, A., Loukachevitch, L. V., Kozekov, I. D., Angel, K. C., Rizzo, C. J., Egli, M., and Guengerich, F. P. (2005) DNA adduct bypass polymerization by *Sulfolobus solfataricus* DNA polymerase Dpo4: analysis and crystal structures of multiple base pair substitution and frameshift products with the adduct 1,N^2-ethenoguanine. *J. Biol. Chem.* **280,** 29750–29764
34. Maddukuri, L., Eoff, R. L., Choi, J. Y., Rizzo, C. J., Guengerich, F. P., and Marnett, L. J. (2010) *In vitro* bypass of the major malondialdehyde- and base propenal-derived DNA adduct by human Y-family DNA polymerases κ, ι, and Rev1. *Biochemistry* **49,** 8415–8424
35. Kotapati, S., Maddukuri, L., Wickramaratne, S., Seneviratne, U., Goggin, M., Pence, M. G., Villalta, P., Guengerich, F. P., Marnett, L., and Tretyakova, N. (2012) Translesion synthesis across 1,N^6-(2-hydroxy-3-hydroxymethylpropan-1,3-diyl)-2′-deoxyadenosine (1,N^6-γ-HMHP-dA) adducts by human and archebacterial DNA polymerases. *J. Biol. Chem.* **287,** 38800–38811
36. Wickramaratne, S., Boldry, E. J., Buehler, C., Wang, Y. C., Distefano, M. D., and Tretyakova, N. Y. (2015) Error-prone translesion synthesis past DNA-peptide cross-links conjugated to the major groove of DNA via C5 of thymidine. *J. Biol. Chem.* **290,** 775–787
37. Lior-Hoffmann, L., Ding, S., Geacintov, N. E., Zhang, Y., and Broyde, S. (2014) Structural and dynamic characterization of polymerase κ's minor groove lesion processing reveals how adduct topology impacts fidelity. *Biochemistry* **53,** 5683–5691
38. Lone, S., Townson, S. A., Uljon, S. N., Johnson, R. E., Brahma, A., Nair, D. T., Prakash, S., Prakash, L., and Aggarwal, A. K. (2007) Human DNA polymerase κ encircles DNA: implications for mismatch extension and lesion bypass. *Mol. Cell* **25,** 601–614
39. Woodgate, R. (1999) A plethora of lesion-replicating DNA polymerases. *Genes Dev.* **13,** 2191–2195
40. Friedberg, E. C., Lehmann, A. R., and Fuchs, R. P. (2005) Trading places: how do DNA polymerases switch during translesion DNA synthesis? *Mol. Cell* **18,** 499–505
41. Lehmann, A. R., Niimi, A., Ogi, T., Brown, S., Sabbioneda, S., Wing, J. F., Kannouche, P. L., and Green, C. M. (2007) Translesion synthesis: Y-family polymerases and the polymerase switch. *DNA Repair* **6,** 891–899
42. Huen, M. S., and Chen, J. (2008) The DNA damage response pathways: at the crossroad of protein modifications. *Cell Res.* **18,** 8–16
43. Sale, J. E., Lehmann, A. R., and Woodgate, R. (2012) Y-family DNA polymerases and their role in tolerance of cellular DNA damage. *Nat. Rev. Mol. Cell Biol.* **13,** 141–152
44. Burgers, P. M., Koonin, E. V., Bruford, E., Blanco, L., Burtis, K. C., Christman, M. F., Copeland, W. C., Friedberg, E. C., Hanaoka, F., Hinkle, D. C., Lawrence, C. W., Nakanishi, M., Ohmori, H., Prakash, L., Prakash, S., Reynaud, C. A., Sugino, A., Todo, T., Wang, Z., Weill, J. C., and Woodgate, R. (2001) Eukaryotic DNA polymerases: proposal for a revised nomenclature. *J. Biol. Chem.* **276,** 43487–43490
45. Ohmori, H., Friedberg, E. C., Fuchs, R. P., Goodman, M. F., Hanaoka, F., Hinkle, D., Kunkel, T. A., Lawrence, C. W., Livneh, Z., Nohmi, T., Prakash, L., Prakash, S., Todo, T., Walker, G. C., Wang, Z., and Woodgate, R. (2001) The Y-family of DNA polymerases. *Mol. Cell* **8,** 7–8
46. Waters, L. S., Minesinger, B. K., Wiltrout, M. E., D'Souza, S., Woodruff, R. V., and Walker, G. C. (2009) Eukaryotic translesion polymerases and their roles and regulation in DNA damage tolerance. *Microbiol. Mol. Biol Rev.* **73,** 134–154
47. Marini, F., Kim, N., Schuffert, A., and Wood, R. D. (2003) POLN, a nuclear PolA family DNA polymerase homologous to the DNA cross-link sensitivity protein Mus308. *J. Biol. Chem.* **278,** 32014–32019
48. McCulloch, S. D., and Kunkel, T. A. (2008) The fidelity of DNA synthesis by eukaryotic replicative and translesion synthesis polymerases. *Cell Res.* **18,** 148–161
49. Friedberg, E. C. (2005) Suffering in silence: the tolerance of DNA damage. *Nat. Rev. Mol. Cell Biol.* **6,** 943–953
50. Yang, W. (2005) Portraits of a Y-family DNA polymerase. *FEBS Lett.* **579,** 868–872
51. Yang, W., and Woodgate, R. (2007) What a difference a decade makes: insights into translesion DNA synthesis. *Proc. Natl. Acad. Sci. U.S.A.* **104,** 15591–15598
52. Mailand, N., Gibbs-Seymour, I., and Bekker-Jensen, S. (2013) Regulation of PCNA-protein interactions for genome stability. *Nat. Rev. Mol. Cell Biol.* **14,** 269–282

53. Matsuda, T., Bebenek, K., Masutani, C., Hanaoka, F., and Kunkel, T. A. (2000) Low fidelity DNA synthesis by human DNA polymerase η. *Nature* **404,** 1011–1013
54. Goodman, M. F. (2002) Error-prone repair DNA polymerases in prokaryotes and eukaryotes. *Annu. Rev. Biochem.* **71,** 17–50
55. Prakash, S., Johnson, R. E., and Prakash, L. (2005) Eukaryotic translesion synthesis DNA polymerases: specificity of structure and function. *Annu. Rev. Biochem.* **74,** 317–353
56. Kuo, H. K., Griffith, J. D., and Kreuzer, K. N. (2007) 5-Azacytidine induced methyltransferase-DNA adducts block DNA replication *in vivo*. *Cancer Res.* **67,** 8248–8254
57. Loeber, R., Michaelson, E., Fang, Q., Campbell, C., Pegg, A. E., and Tretyakova, N. (2008) Cross-linking of the DNA repair protein O^6-alkylguanine DNA alkyltransferase to DNA in the presence of antitumor nitrogen mustards. *Chem. Res. Toxicol.* **21,** 787–795
58. Kelland, L. (2007) The resurgence of platinum-based cancer chemotherapy. *Nat. Rev. Cancer* **7,** 573–584
59. Wheate, N. J., Walker, S., Craig, G. E., and Oun, R. (2010) The status of platinum anticancer drugs in the clinic and in clinical trials. *Dalton Trans.* **39,** 8113–8127
60. Hall, A. G., and Tilby, M. J. (1992) Mechanisms of action of, and modes of resistance to, alkylating agents used in the treatment of haematological malignancies. *Blood Rev.* **6,** 163–173
61. Wang, C. C., Li, J., Teo, C. S., and Lee, T. (1999) The delivery of BCNU to brain tumors. *J. Control Release* **61,** 21–41
62. Gilman, A., and Philips, F. S. (1946) The biological actions and therapeutic applications of the β-chloroethyl amines and sulfides. *Science* **103,** 409–436
63. Nakano, T., Morishita, S., Katafuchi, A., Matsubara, M., Horikawa, Y., Terato, H., Salem, A. M., Izumi, S., Pack, S. P., Makino, K., and Ide, H. (2007) Nucleotide excision repair and homologous recombination systems commit differentially to the repair of DNA-protein crosslinks. *Mol. Cell* **28,** 147–158
64. Kumari, A., Minko, I. G., Smith, R. L., Lloyd, R. S., and McCullough, A. K. (2010) Modulation of UvrD helicase activity by covalent DNA-protein cross-links. *J. Biol. Chem.* **285,** 21313–21322
65. Minko, I. G., Zou, Y., and Lloyd, R. S. (2002) Incision of DNA-protein crosslinks by UvrABC nuclease suggests a potential repair pathway involving nucleotide excision repair. *Proc. Natl. Acad. Sci. U.S.A.* **99,** 1905–1909
66. Quievryn, G., and Zhitkovich, A. (2000) Loss of DNA-protein crosslinks from formaldehyde-exposed cells occurs through spontaneous hydrolysis and an active repair process linked to proteosome function. *Carcinogenesis* **21,** 1573–1580
67. Baker, D. J., Wuenschell, G., Xia, L., Termini, J., Bates, S. E., Riggs, A. D., and O'Connor, T. R. (2007) Nucleotide excision repair eliminates unique DNA-protein cross-links from mammalian cells. *J. Biol. Chem.* **282,** 22592–22604
68. Reardon, J. T., Cheng, Y., and Sancar, A. (2006) Repair of DNA-protein cross-links in mammalian cells. *Cell Cycle* **5,** 1366–1370
69. Yamanaka, K., Minko, I. G., Takata, K., Kolbanovskiy, A., Kozekov, I. D., Wood, R. D., Rizzo, C. J., and Lloyd, R. S. (2010) Novel enzymatic function of DNA polymerase ν in translesion DNA synthesis past major groove DNA-peptide and DNA-DNA cross-links. *Chem. Res. Toxicol.* **23,** 689–695
70. Minko, I. G., Yamanaka, K., Kozekov, I. D., Kozekova, A., Indiani, C., O'Donnell, M. E., Jiang, Q., Goodman, M. F., Rizzo, C. J., and Lloyd, R. S. (2008) Replication bypass of the acrolein-mediated deoxyguanine DNA-peptide cross-links by DNA polymerases of the DinB family. *Chem. Res. Toxicol.* **21,** 1983–1990
71. Levine, R. L., Miller, H., Grollman, A., Ohashi, E., Ohmori, H., Masutani, C., Hanaoka, F., and Moriya, M. (2001) Translesion DNA synthesis catalyzed by human pol η and pol κ across 1,N^6-ethenodeoxyadenosine. *J. Biol. Chem.* **276,** 18717–18721
72. Zhao, L., Pence, M. G., Christov, P. P., Wawrzak, Z., Choi, J. Y., Rizzo, C. J., Egli, M., and Guengerich, F. P. (2012) Basis of miscoding of the DNA adduct N^2,3-ethenoguanine by human Y-family DNA polymerases. *J. Biol. Chem.* **287,** 35516–35526
73. Patra, A., Su, Y., Zhang, Q., Johnson, K. M., Guengerich, F. P., and Egli, M. (2016) Structural and kinetic analysis of miscoding opposite the DNA adduct 1,N^6-ethenodeoxyadenosine by human translesion polymerase η. *J. Biol. Chem.* **291,** 14134–14145
74. Cho, S. H., and Guengerich, F. P. (2013) Replication past the butadiene diepoxide-derived DNA adduct *S*-[4-(N^6-deoxyadenosinyl)-2,3-dihydroxybutyl]glutathione by DNA polymerases. *Chem. Res. Toxicol.* **26,** 1005–1013
75. Ganguly, M., Wang, F., Kaushik, M., Stone, M. P., Marky, L. A., and Gold, B. (2007) A study of 7-deaza-2′-deoxyguanosine 2′-deoxycytidine base pairing in DNA. *Nucleic Acids Res.* **35,** 6181–6195
76. Kowal, E. A., Ganguly, M., Pallan, P. S., Marky, L. A., Gold, B., Egli, M., and Stone, M. P. (2011) Altering the electrostatic potential in the major groove: thermodynamic and structural characterization of 7-deaza-2′-deoxyadenosine:dT base pairing in DNA. *J. Phys. Chem. B* **115,** 13925–13934
77. Räschle, M., Knipscheer, P., Enoiu, M., Angelov, T., Sun, J., Griffith, J. D., Ellenberger, T. E., Schärer, O. D., and Walter, J. C. (2008) Mechanism of replication-coupled DNA interstrand crosslink repair. *Cell* **134,** 969–980
78. Enoiu, M., Ho, T. V., Long, D. T., Walter, J. C., and Schärer, O. D. (2012) Construction of plasmids containing site-specific DNA interstrand crosslinks for biochemical and cell biological studies. *Methods Mol. Biol.* **920,** 203–219
79. Roy, U., and Schärer, O. D. (2016) Involvement of translesion synthesis DNA polymerases in DNA interstrand crosslink repair. *DNA Repair* **44,** 33–41
80. Rechkoblit, O., Zhang, Y., Guo, D., Wang, Z., Amin, S., Krzeminsky, J., Louneva, N., and Geacintov, N. E. (2002) *trans*-Lesion synthesis past bulky benzo[*a*]pyrene diol epoxide N^2-dG and N^6-dA lesions catalyzed by DNA bypass polymerases. *J. Biol. Chem.* **277,** 30488–30494
81. Jia, L., Geacintov, N. E., and Broyde, S. (2008) The N-clasp of human DNA polymerase κ promotes blockage or error-free bypass of adenine- or guanine-benzo[*a*]pyrenyl lesions. *Nucleic Acids Res.* **36,** 6571–6584
82. Yang, W. (2014) An overview of Y-family DNA polymerases and a case study of human DNA polymerase η. *Biochemistry* **53,** 2793–2803
83. Fedtke, N., Boucheron, J. A., Walker, V. E., and Swenberg, J. A. (1990) Vinyl chloride-induced DNA adducts. II: Formation and persistence of 7-(2′-oxoethyl)guanine and N^2,3-ethenoguanine in rat tissue DNA. *Carcinogenesis* **11,** 1287–1292
84. Patra, A., Nagy, L. D., Zhang, Q., Su, Y., Müller, L., Guengerich, F. P., and Egli, M. (2014) Kinetics, structure, and mechanism of 8-oxo-7,8-dihydro-2′-deoxyguanosine bypass by human DNA polymerase η. *J. Biol. Chem.* **289,** 16867–16882
85. Irimia, A., Eoff, R. L., Guengerich, F. P., and Egli, M. (2009) Structural and functional elucidation of the mechanism promoting error-prone synthesis by human DNA polymerase κ opposite the 7,8-dihydro-8-oxo-2′-deoxyguanosine adduct. *J. Biol. Chem.* **284,** 22467–22480
86. Chung, J. A., Wollack, J. W., Hovlid, M. L., Okesli, A., Chen, Y., Mueller, J. D., Distefano, M. D., and Taton, T. A. (2009) Purification of prenylated proteins by affinity chromatography on cyclodextrin-modified agarose. *Anal. Biochem.* **386,** 1–8